

12  
2-19-92 JS (1)

PNL-7816

UC-721

---

**Corrosion Studies of Carbon Steel  
Under Impinging Jets of Simulated  
Slurries of Neutralized Current Acid  
Waste (NCAW) and Neutralized  
Cladding Removal Waste (NCRW)**

H. D. Smith  
M. R. Elmore

---

January 1992

Prepared for U.S. Department of Energy  
under Contract DE-AC06-76RI.O 1830

Pacific Northwest Laboratory  
Operated for the U.S. Department of Energy  
by Battelle Memorial Institute



PNL-7816

## DISCLAIMER

This report was prepared as an account of work sponsored by an agency of the United States Government. Neither the United States Government nor any agency thereof, nor Battelle Memorial Institute, nor any of their employees, makes **any warranty, expressed or implied, or assumes any legal liability or responsibility for the accuracy, completeness, or usefulness of any information, apparatus, product, or process disclosed, or represents that its use would not infringe privately owned rights.** Reference herein to any specific commercial product, process, or service by trade name, trademark, manufacturer, or otherwise does not necessarily constitute or imply its endorsement, recommendation, or favoring by the United States Government or any agency thereof, or Battelle Memorial Institute. The views and opinions of authors expressed herein do not necessarily state or reflect those of the United States Government or any agency thereof.

PACIFIC NORTHWEST LABORATORY  
*operated by*  
BATTELLE MEMORIAL INSTITUTE  
*for the*  
UNITED STATES DEPARTMENT OF ENERGY  
*under Contract DE-AC06-76RLO 1830*

Printed in the United States of America

Available to DOE and DOE contractors from the  
Office of Scientific and Technical Information, P.O. Box 62, Oak Ridge, TN 37831;  
prices available from (615) 576-8401. FTS 625-001.

Available to the public from the National Technical Information Service,  
U.S. Department of Commerce, 5285 Port Royal Rd., Springfield, VA 22161.

PNL--7816

DE92 007605

CORROSION STUDIES OF CARBON STEEL UNDER  
IMPINGING JETS OF SIMULATED SLURRIES OF  
NEUTRALIZED CURRENT ACID WASTE (NCAW) AND  
NEUTRALIZED CLADDING REMOVAL WASTE (NCRW)

H. D. Smith  
M. R. Elmore

January 1992

Prepared for  
the U.S. Department of Energy  
under Contract DE-AC06-76RLO 1830

Pacific Northwest Laboratory  
Richland, Washington 99352

MASTER

DB

## ABSTRACT

Plans for the disposal of radioactive liquid and solid wastes presently stored in double-shell tanks at the Hanford Site call for retrieval and processing of the waste to create forms suitable for permanent disposal. Waste will be retrieved from a tank using a submerged slurry pump in conjunction with one or more rotating slurry jet mixer pumps. Pacific Northwest Laboratory (PNL) has conducted tests using simulated waste slurries to assess the effects of an impinging slurry jet on the corrosion rate of the tank wall and floor, an action that could potentially compromise the tank's structural integrity. Corrosion processes were investigated on a laboratory scale with a simulated neutralized cladding removal waste (NCRW) slurry and in a subsequent test with simulated neutralized current acid waste (NCAW) slurry. The test slurries simulated the actual NCRW and NCAW both chemically and physically. The tests simulated those conditions expected to exist in the respective double-shell tanks during waste retrieval operations. Results of both tests indicate that, because of the action of the mixer pump slurry jets, the waste retrieval operations proposed for NCAW and NCRW will moderately accelerate corrosion of the tank wall and floor. Based on the corrosion of initially unoxidized test specimens, and the removal of corrosion products from those specimens, the maximum time-averaged corrosion rates of carbon steel in both waste simulants for the length of the test was ~4 mil/yr. The protective oxide layer that exists in each storage tank is expected to inhibit corrosion of the carbon steel.

## SUMMARY

Plans are being developed to dispose of several million gallons of radioactive liquid and solid wastes stored in double-shell tanks at the Hanford Site. These wastes will be retrieved and processed to create waste forms suitable for permanent disposal. Waste will be retrieved from a tank using a submerged slurry pump in conjunction with one or more rotating slurry jet mixer pumps. However, there is concern that the action of the jets in resuspending the settled solids may accelerate corrosion of the tank wall and floor. If the corrosion rates observed during testing with simulated wastes are high enough to compromise the structural integrity of the tanks, then mixing pumps may not be the best alternative for waste retrieval and a change in retrieval strategy may be required. An unacceptable corrosion rate would depend on the corrosion allowance originally designed into the tank, the estimated amount of corrosion experienced while the tank was in service, the time needed to retrieve the waste, and any future plans for the tank.

Pacific Northwest Laboratory (PNL) has conducted corrosion tests with simulated waste slurries to investigate the likelihood and magnitude of accelerated corrosion of the double-shell tanks during retrieval operations. In FY 1989, corrosion processes were investigated on a laboratory scale with a simulated neutralized cladding removal waste (NCRW) slurry. Lessons learned from this test were incorporated into a subsequent test conducted in FY 1990 with simulated neutralized current acid waste (NCAW) slurry. The results of these two scoping tests are reported here.

The principal objective of these corrosion tests was to assess the effects of an impinging slurry jet on the corrosion rate of the tank wall and floor. More specifically, the testing determined the magnitude of accelerated corrosion of A-537 carbon steel, the type of steel used to fabricate the majority of the double-shell tanks, from impinging jets of caustic slurries as compared to expected corrosion rates under normal waste storage conditions.

The apparatus used for the NCAW and NCRW corrosion tests reported herein simulated those conditions anticipated in the respective double-shell tanks during waste retrieval operations as accurately as possible by producing the

same direct impingement flow velocities (although the indirect impingement was not quantified in the NCAW test); temperatures; and in the case of the NCAW test, jet impingement times expected during waste retrieval. The test slurries simulated the actual NCRW and NCAW both chemically and physically (i.e., vol% solids and abrasivity).

Three slurry flow velocities were used for each test. For the NCRW test, the velocities tested were 3.6, 14.4, and 54.5 ft/s, with the high velocity approximating the calculated exit velocity of the slurry from the pump nozzle. For the NCAW test, the high velocity of 15 ft/s represented the maximum slurry velocity expected at the tank wall for a two-pump arrangement and a nozzle discharge parameter of  $U_0 D = 29.4 \text{ ft}^2/\text{s}$ . A slow slurry velocity of 4 ft/s and an intermediate velocity of 8 ft/s were also tested. The velocities chosen for the NCAW test more closely represent the conditions expected at the tank wall during the slurry retrieval operations.

The temperature of the waste in the double-shell tanks is normally maintained at  $\sim 140^\circ\text{F}$  ( $60^\circ\text{C}$ ), but the power expended by the mixer pumps during sludge resuspension is expected to cause the temperature of the slurry to climb to near its boiling point during retrieval. Hence, the test temperature of  $180^\circ\text{F}$  ( $82^\circ\text{C}$ ) for the NCRW test was a compromise between the need to reduce evaporation of water from the slurry and to investigate corrosion at a temperature closer to that expected during retrieval. Redesigning the test vessel allowed the NCAW test to be conducted at a temperature near the slurry's boiling point ( $103^\circ\text{C}$ ).

The rotating slurry mixer pump(s) will cause the slurry jets to strike a particular point on the tank floor or wall in a cyclic manner about 10% of the pump's total operating time. In the earlier NCRW test, the coupons were exposed to the jets for the length of the test. The equipment for the NCAW test was modified to simulate the cyclic impact of the jets on the tank walls by moving the coupons into and out of the flows of the fixed jets on a repeating cycle of 0.5 minute in one position and 4.5 minutes in the switched position. However, the nature of the slurry flow in the indirect impingement position was not known. Carbon steel coupons were also suspended in a

non-flowing location in the slurry of each test to serve as control coupons for comparison and correction of the calculated corrosion rates that can be attributed to impinging jets.

The NCRW test was conducted for 107 days of coupon exposure to the slurry. The coupons were examined during the NCRW test at intervals of every week for the first two weeks and then every two weeks. The NCAW test was conducted for 150 days of exposure to the slurry. The coupons were examined during the NCAW test at exposure times of 7, 16, 30, 42, 51, 92, 122, and 150 days from the beginning of the test. The time interval between examinations for the NCAW test was extended as the corrosion response of the coupons was defined and tended toward a presumed constant reaction rate.

Results of both tests indicate that, because of the action of the mixer pump slurry jets, the waste retrieval operations proposed for NCAW and NCRW will moderately accelerate corrosion of the tank wall and floor. Based on the corrosion of initially unoxidized test specimens, and the removal of corrosion products from those specimens, the maximum time-averaged corrosion rates of carbon steel in both waste simulants for the length of the test was ~4 mil/yr.

For the NCRW test, a time-averaged corrosion rate of 2.8 mil/yr was calculated for a slurry jet velocity of 14.4 ft/s (4.4 m/s). A time-averaged corrosion rate of ~4 mil/yr was calculated for the highest jet velocity tested for the NCAW test [15 ft/s (4.6 m/s)]. In the NCAW test, the 4-mil/yr result was found for the coupon that was in the jet only ~10% of the time. This result was unexpected, and is discussed further in the body of this report. Both rates are based on the final weight after the remaining oxide layer was removed from the coupon. These corrosion values are an average rate for the total test that includes the effect of an initially higher rate before achieving a presumed steady-state rate. As such, they may be considered conservative maximum values. They compare with a rate of ~0.3 mil/yr measured for coupons in a non-flow region of both test vessels but otherwise similar conditions. The maximum total base metal loss for the 150-day NCAW test was ~1.6 mils.

A discussion of the actual waste storage and retrieval conditions is appropriate to relate the scoping test results to expected corrosion in the

double-shell tanks during waste retrieval. First, the tank surfaces are heavily oxidized following fabrication as a result of the stress relief process. Since their fabrication, the tanks have contained corrosive wastes that have probably further increased the thickness of the oxide layers. The effect of this oxide layer is to inhibit corrosion by creating a diffusion barrier between the metal and bulk solution.

Analysis of the weight loss data from the NCAW coupons with the oxide layer intact indicates it is likely that a lower corrosion rate of 2.5 mil/yr or less may occur over the long term during actual waste mobilization and retrieval operations (see Table 5.4). Similar results are seen for the NCRW coupons--1 to 2.2 mil/yr based on weight loss during the last test interval. This rate is somewhat less. However, there are uncertainties in the rates of potentially competing mechanisms in the corrosion phenomenon. For example, the observed weight changes during test intervals without removing the oxide films is from a combination of material lost from the specimen and material incorporated into the oxide layer. The combined effect of this summation can be measured, but the magnitude of either term is indeterminate. Therefore, these lower values for corrosion rates, although potentially closer to reality, could not be substantiated with the design of the current scoping test, since the design depends on the assumption that the oxide film had reached a steady-state condition.

CONTENTS

ABSTRACT . . . . .	iii
SUMMARY . . . . .	v
1.0 INTRODUCTION . . . . .	1.1
1.1 BACKGROUND . . . . .	1.4
1.2 OBJECTIVES . . . . .	1.4
2.0 CONCLUSIONS AND RECOMMENDATIONS . . . . .	2.1
3.0 CORROSION THEORY . . . . .	3.1
3.1 CORROSION OF CARBON STEEL . . . . .	3.2
3.2 CORROSION MODELS . . . . .	3.5
3.3 FLOW PATTERNS IN IMPINGING ROUND JETS . . . . .	3.7
4.0 TEST APPROACH . . . . .	4.1
4.1 TEST APPARATUS . . . . .	4.3
4.1.1 NCRW Test Apparatus . . . . .	4.3
4.1.2 NCAW Test Apparatus . . . . .	4.4
4.2 TEST MATERIALS . . . . .	4.8
4.2.1 Simulated NCRW Slurry . . . . .	4.8
4.2.2 Simulated NCAW Slurry . . . . .	4.9
4.2.3 Carbon Steel Test Coupons . . . . .	4.9
4.3 CORROSION TEST PARAMETERS . . . . .	4.11
4.3.1 Jet Velocities . . . . .	4.12
4.3.2 Temperature . . . . .	4.12
4.3.3 Impingement Times . . . . .	4.13
4.3.4 Air Sparge . . . . .	4.13

4.4	TEST PROCEDURES . . . . .	4.15
4.4.1	Coupon Preparation . . . . .	4.15
4.4.2	Test Protocol . . . . .	4.15
4.4.3	Coupon Cleaning and Examination . . . . .	4.16
5.0	TEST RESULTS . . . . .	5.1
5.1	EXPECTED RESULTS . . . . .	5.1
5.1.1	Mechanical Processes Causing Material Loss . . . . .	5.1
5.1.2	Chemical "Corrosion" Dominant Processes . . . . .	5.2
5.2	INTERIM TEST RESULTS . . . . .	5.6
5.2.1	Control Coupons . . . . .	5.7
5.2.2	Impingement Coupons . . . . .	5.8
5.3	FINAL TEST RESULTS . . . . .	5.16
5.3.1	Control Coupons . . . . .	5.17
5.3.2	Impingement Coupons . . . . .	5.18
6.0	DISCUSSION OF RESULTS FROM IMPINGEMENT CORROSION TESTS . . . . .	6.1
6.1	SIMILARITIES AND CONTRASTS BETWEEN NCAW AND NCRW TESTS . . . . .	6.1
6.2	SIMILARITIES AND CONTRASTS BETWEEN NCRW AND NCAW TEST RESULTS . . . . .	6.4
6.3	INTERPRETATION OF INTERIM WEIGHT CHANGE OBSERVATIONS . . . . .	6.9
6.4	CONCLUSIONS AND RECOMMENDATIONS FOR FUTURE TESTS . . . . .	6.13
7.0	REFERENCES . . . . .	7.1
APPENDIX A	- COUPON DIMENSIONS AND WEIGHT MEASUREMENTS . . . . .	A.1

## FIGURES

1.1	Carbon Steel Double-Shell Tanks Under Construction at a Hanford Tank Farm . . . . .	1.1
1.2	Photograph from Inside Double-Shell Tank 241-AZ-101 . . . . .	1.2
1.3	Proposed Waste Retrieval Method Using Mixer Pumps to Resuspend Settled Solids in Double-Shell Tanks and a Transfer Pump to Remove the Waste Slurry . . . . .	1.4
3.1	Model for Corrosion of Carbon Steel in High-Temperature Water Environment Showing Diffusing Species on Left Side of Illustration and Typical Reactions Forming a Film on Right Side . . . . .	3.2
3.2	Experimental Solubilities of Magnetite at 423 and 373 K and 779 $\mu\text{mole/kg H}_2$ . . . . .	3.4
3.3	Impinging Fluid Jet Showing Flow Characterized by Three Principal Regions: 1) Free Jet Region, 2) Impingement Region, and 3) Wall Jet Region . . . . .	3.8
4.1	Nozzle and Impingement Coupon, and Illustration of Test Apparatus Used for the NCRW Jet Impingement Corrosion Test . . . . .	4.3
4.2	Test Apparatus Used for NCAW Jet Impingement Corrosion Test . . . . .	4.5
4.3	ASTM A-537 Carbon Steel Coupons Used for the NCRW Corrosion Test and the NCAW Test . . . . .	4.7
5.1	Two Examples of Hypothetical Weight Change Rate Versus Time Dependencies for Steel Corrosion Observations . . . . .	5.4
5.2	Typical Areas of the Surfaces of Two NCAW Control Specimens Before Oxide Removal . . . . .	5.9
5.3	Impingement Coupon and Method Used to Calculate "Adjusted" Corrosion Rate . . . . .	5.10
5.4	NCAW Impingement Coupons Exposed to Low-Velocity Jets Before Oxide Removal . . . . .	5.12
5.5	NCAW Impingement Coupons Exposed to Medium-Velocity Jets Before Oxide Removal . . . . .	5.13
5.6	NCAW Impingement Coupons Exposed to High-Velocity Jets Before Oxide Removal . . . . .	5.14

5.7	Typical Surface Area of NCAW Control Coupon Following the Cleaning Process . . . . .	5.18
6.1	Probable Flow Pattern for NCAW Slurry Jet . . . . .	6.3
6.2	Post-Cleaning Corrosion Rates as a Function of Jet Velocity . . .	6.6
6.3	Correlation of Time-Averaged Corrosion Rates with Oxide Film Mass . . . . .	6.7
6.4	Plots of Measured Weight Loss Rates for the Control Coupons from the NCAW and NCRW Corrosion Tests . . . . .	6.10
6.5	Plots of Measured Weight Loss Rates for the Impingement Coupons from the NCAW and NCRW Corrosion Tests . . . . .	6.11

TABLES

4.1	Composition of Simulated NCRW and Simulated NCAW Slurries . . . . .	4.8
4.2	Pretest Weights and Dimensions for the NCRW and NCAW Corrosion Test Coupons . . . . .	4.10
4.3	Comparison of Chemical Compositions for A-515 Steel, ASTM A-537 Carbon Steel, and Erosion-Corrosion Test Material . . . . .	4.11
5.1	Cumulative Weight Loss as a Function of Time for the NCRW and NCAW Control Coupons . . . . .	5.7
5.2	Comparison of Adjusted Cumulative Weight Loss as a Function of Time for the NCRW and NCAW Impingement Coupons . . . . .	5.11
5.3	Summary of Data for Control Coupons from NCRW and NCAW Tests . . .	5.17
5.4	Final Adjusted Weight Losses and Time-Averaged Corrosion Rates for the Impingement Coupons . . . . .	5.19
6.1	Comparison of NCRW and NCAW Corrosion Test Parameters . . . . .	6.1
6.2	Summary of Results from NCRW and NCAW Corrosion Tests . . . . .	6.5

## 1.0 INTRODUCTION

Several million gallons of radioactive liquid and solid wastes are stored in double-shell tanks (DSTs) at the Hanford Site. The DSTs were constructed at Hanford beginning in the late 1960s to provide interim storage for radioactive liquid defense wastes produced at Hanford during various fuel processing operations. Figure 1.1 shows a group of the DSTs, or a "tank farm," under construction.



FIGURE 1.1. Carbon Steel Double-Shell Tanks Under Construction at a Hanford Tank Farm

Before wastes are stored in the DSTs, they are neutralized with a caustic solution to a pH greater than ~12 and are chemically inhibited by the addition of a nitrite ion to minimize corrosion of the carbon steel. This neutralization produces precipitates, primarily hydroxide complexes, that eventually separate from the rest of the liquid. Figure 1.2 shows the inside of a

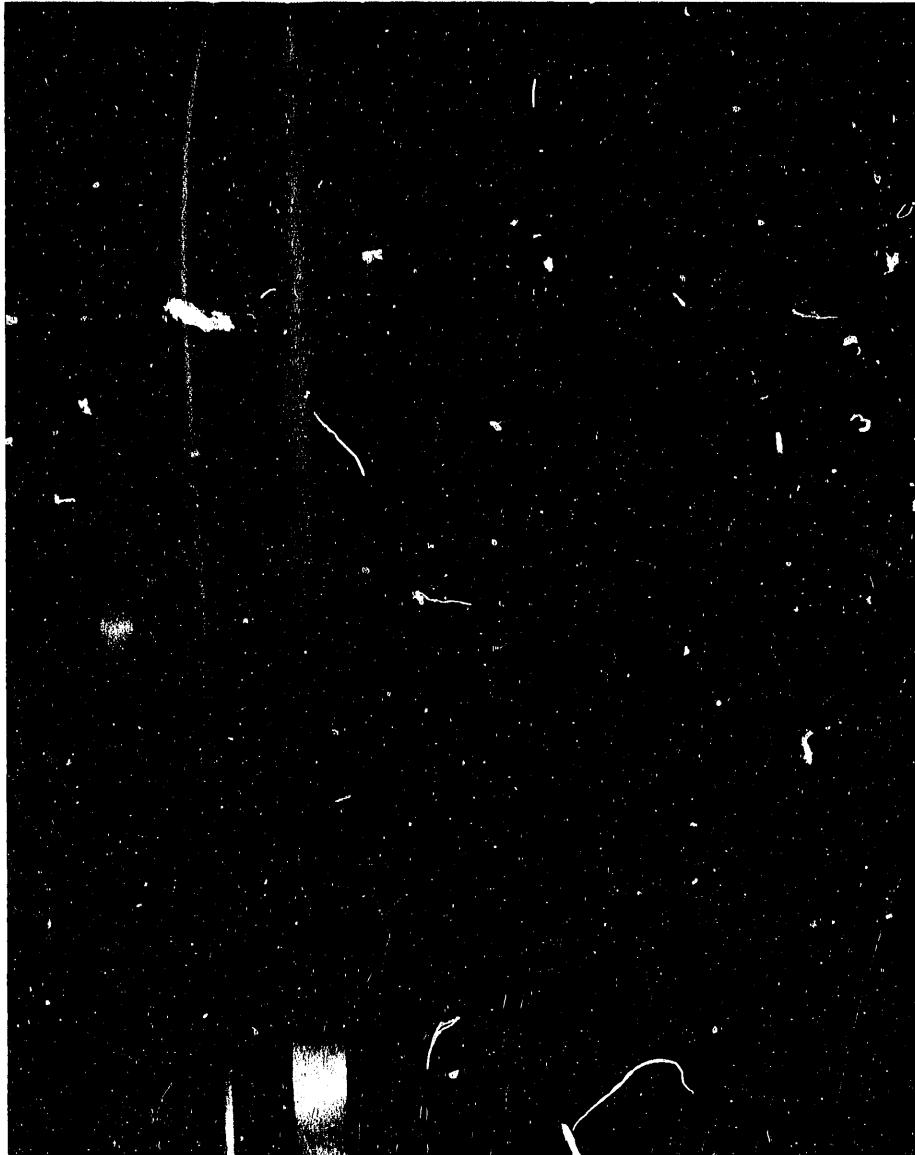


FIGURE 1.2. Photograph from Inside Double-Shell Tank 241-AZ-101. Tank is partially filled with neutralized current acid waste.

DST that is partially filled with "neutralized" waste. These wastes will be retrieved and processed to create waste forms suitable for permanent disposal.

Solids in some of these tanks have been settling for many years, creating sludge layers on the tank floors. The solids must be resuspended in the supernatant liquids before waste retrieval operations can begin. Waste will be retrieved from a tank using a submerged slurry/transfer pump in conjunction with one or more rotating slurry jet mixer pumps. Each mixer pump will generate two opposing high-volume jets of fluid and will direct those jets at the settled solids. Figure 1.3 shows the proposed retrieval method using mixer pumps to resuspend the settled solids and a transfer pump to remove the slurry.

Westinghouse Hanford Company (WHC) is concerned that the action of the jets in resuspending the settled solids may accelerate corrosion of the tank wall and floor. To investigate this concern, Pacific Northwest Laboratory (PNL)<sup>(a)</sup> has conducted scoping tests of tank corrosion using simulated waste slurries to assess the likelihood and magnitude of accelerated corrosion of the DSTs during waste retrieval.

Corrosion processes have been investigated by PNL at this time using two types of simulated Hanford waste: neutralized cladding removal waste (NCRW) and neutralized current acid waste (NCAW). Tests with NCRW were initiated in FY 1988 and completed in FY 1989; tests with NCAW were performed in FY 1990. The results of the NCAW and NCRW testing are reported and compared in this report.

## 1.1 BACKGROUND

The Hanford Site Environmental Restoration and Waste Management Technology Plan (HSERWMTP) (Anantamula 1990) for calendar year 1989 describes 28 DSTs in service at the Hanford Site with a total capacity of ~31 M gal (118,400 m<sup>3</sup>). Within these tanks, approximately 21 M gal (78,000 m<sup>3</sup>) of DST waste had accumulated as of December 31, 1988. More wastes are expected.

---

(a) Pacific Northwest Laboratory is operated by Battelle Memorial Institute for the U.S. Department of Energy under contract DE-AC06-76RLO 1830.

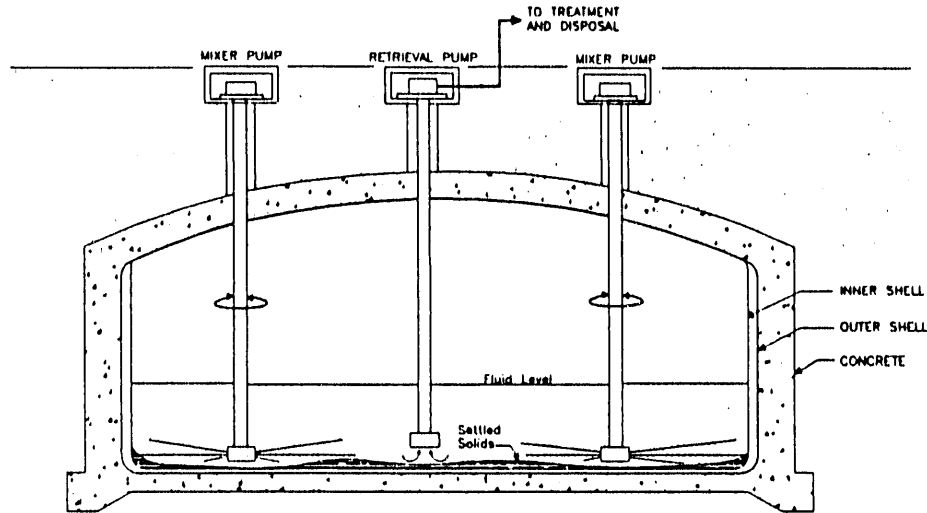


**FIGURE 1.3.** Proposed Waste Retrieval Method Using Mixer Pumps to Resuspend Settled Solids in Double-Shell Tanks and a Transfer Pump to Remove the Waste Slurry

Two of the waste types, NCAW and NCRW, have been identified as sources of high-level waste (HLW) fractions. These waste streams are to be retrieved from the DSTs and pretreated at B Plant before they are immobilized. In addition, following waste retrieval and pretreatment, at least one of the DSTs (i.e., 101-AZ) will be used as a holding tank for pretreated waste that will be pumped to the Hanford Waste Vitrification Plant (HWVP).

Several technical issues must still be resolved before implementing the plan to retrieve and immobilize the DST wastes. These issues are summarized in the HSERWMTF (Anantatmula 1990) and include determining retrieval characteristics of the various waste types and developing methods and equipment requirements for mobilizing the sludges and retrieving the wastes. As part of solving the technical issues related to waste retrieval, the concern about possible increased corrosion of the tank walls and floors is being addressed.

## 1.2 OBJECTIVES

The principal objective of the corrosion testing task in the DST Retrieval Project is to assess the effects of impinging slurry jets on the

corrosion rate of the carbon steel used to fabricate some of the DSTs. Specifically, the purpose of the scoping tests was to indicate how much faster the steel corrodes when it is impinged by jets of caustic slurries (simulating the mixer pump action with mobilized DST wastes) than it does under normal, more stagnant waste storage conditions.

A specific objective of the testing was to simulate, as closely as practicable, the conditions in the waste tank that are most significant to corrosion during waste retrieval operations: 1) the test slurries must adequately simulate the actual tank wastes, both chemically and physically; 2) the test coupon material must match the material used to fabricate the tanks; and 3) the slurry temperature and velocity of the slurry jets striking the test coupons must match anticipated conditions in the waste tanks. The velocity of the slurry jet is determined by the desired cleaning effectiveness for the retrieval operations. The cleaning effectiveness, or effective cleaning radius (ECR), of the mixer pump is proportional to the product of the exit velocity ( $U_0$ ) and nozzle diameter (D), but is also dependent on the rheological properties of the sludge to be resuspended. These scoping tests simulated all major conditions except the effects of angular impingement and non-direct impingement flows.

If the corrosion rates observed during testing with simulated wastes are unacceptably high such that waste retrieval operations might compromise the structural integrity of the tanks, the mixing pumps may not be the best alternative and a change in retrieval strategy may be required. An unacceptable corrosion rate would depend on the corrosion allowance originally designed into the tank, the estimated amount of corrosion experienced while the tank was in service, the time needed to retrieve the waste, and any future plans for the tank.

## 2.0 CONCLUSIONS AND RECOMMENDATIONS

The following items summarize the major conclusions and recommendations drawn from the testing program described in this report.

- Based on data from impinging jet corrosion tests conducted on carbon steel with simulated wastes, waste retrieval operations for NCAW and NCRW are predicted to cause moderately accelerated corrosion of DST tank walls and floors as a result of the action of the mixer pump slurry jets.
- These tests were initiated with clean unoxidized steel specimens, which were then corroded by impinging jets of simulated waste slurries. Time-averaged corrosion rates were determined from measured weight changes occurring over the time of the test. The maximum accelerated corrosion rate determined by this method for the NCAW test was ~4 mil/yr, occurring at the highest jet velocity tested, 15 ft/s (4.6 m/s), and after removal of the accumulated oxide layer. A smaller value, 2.8 mil/yr, was determined for the NCRW test run at 14.4 ft/s (4.4 m/s); however, any direct comparison is not appropriate because of other differences between the two tests. These values are time-averaged corrosion rates, which include the effect of an initially higher rate before a presumed steady-state condition was achieved. The total base metal thickness loss during the NCAW 150-day test was ~1.6 mils, while a surface-averaged loss of 0.82 mils was observed during the 107-day NCRW test.
- Corrosion rates are expected to decrease over time with the accumulation of an oxide layer that presents a barrier to diffusion of reactants and reaction products involved in the corrosion reactions. Analysis of weight loss data from the NCAW coupons after 92 days, assuming the surface oxide layer is unchanging, indicates that a corrosion rate of <2.5 mil/yr would probably occur over the long term during actual waste mobilization operations. However, because of uncertainties in the effects of competing mechanisms occurring in the corrosion phenomenon, lower numbers for both the NCAW and NCRW tests cannot be fully substantiated from the available data. This is particularly true for the NCRW test, so the time-averaged value of 2.8 mil/yr for a slurry velocity of 14.4 ft/s is suggested for use with wastes like the simulated NCRW composition. Following sludge mobilization, while the slurry is being removed from the DSTs, the mixer pump jet velocities may be lowered significantly. If so, the resulting corrosion rate is expected to be less.
- After the NCAW test duration of 150 days, final weight loss measurements (after chemically removing oxide films) for the non-flow (control) coupons produced calculated corrosion rates of ~0.3 mil/yr at ~217°F (103°C). A similar rate was measured for the NCRW control coupons. These values are comparable to other reported corrosion

rates in these types of caustic Hanford wastes (Divine et al. 1985). Because the baseline corrosion rates from the control coupons are comparable to other results with similar solutions, the validity of the corrosion responses of the carbon steel to the simulated NCAW and NCRW slurries are supported.

- Within the bounds of the specific conditions evaluated in this corrosion test, the results are a good estimate of the corrosion that may occur from the mixer pumps in the DSTs operating within the assumed configuration that provided the basis for the test parameters (i.e., two mixer pumps,  $U_0D = 29.4 \text{ ft}^2/\text{s}$ , etc.). However, because of the lack of duplicate coupons or duplicate tests, the uncertainty in the weight loss results and calculated enhanced corrosion rates has not been estimated for the corrosion tests.
- There were significant differences in the test conditions for the two corrosion tests, and in the characteristics of the corrosion films as determined after the tests: 1) temperatures differed by  $35^\circ\text{F}$ ; 2) simulant compositions differed greatly; and 3) the NCRW coupons were continuously exposed to the jets, while the NCAW coupons were switched into and out of the jets. The NCAW impingement coupons had considerably thicker oxide film accumulations than those on the NCRW impingement coupons, while the opposite outcome was observed between the control coupons of the two tests. This suggests that the corrosion film on the coupons in the NCRW simulant consisted of a different oxide structure than that formed on coupons exposed to the NCAW simulant. These factors represent significant differences in the two tests. It is probable that the similarities in the corrosion rates for the static coupons as well as the impingement coupons for these two waste simulants are merely coincidental. The likelihood that corrosion rates for any other likely combination of waste retrieval variables will be the same as indicated by these tests, although possible, is improbable.
- Numerous variables exist in these systems, and some of the variables may have complex interactions. In particular, the effects of temperature and waste composition on corrosion are not as well documented for "flow-type" systems as they are for "static" corrosion systems. Additional testing is needed to clearly understand the corrosion processes that are occurring in these systems so that the results of these tests may be extrapolated to other conditions or waste compositions. Duplicate coupons should be included in plans for future testing to provide a more precise determination of the long-term accelerated corrosion rates expected during waste retrieval.
- Microscopic examination of the NCAW coupons before and after removal of the oxide films indicates that the corrosion mechanism involved in this system is wholly or predominantly uniform corrosion.

Uniform corrosion was assumed for subsequent calculations of baseline (control) corrosion and corrosion rates, and the assumption was supported by photomicrographs.

- The effect of relative impingement time on the corrosion rate of the NCAW samples was inconclusive. The weight loss measurements showed increased weight loss with increased relative impingement time for the low and medium velocities, but weight losses from the high-velocity pair of specimens were reversed from what would be expected (i.e., the short-exposure specimen had higher weight loss than the long-exposure specimen). This result is believed to indicate that the slurry motion in the off-jet position was not as negligible as originally thought, and the trends indicated in Table 6.2 for both long-time in-jet and long-time off-jet positions reflect the kinds of flow washing over the surface of the coupon. Unfortunately, the flow in the off-jet position is undefined but is potentially more active in stimulating corrosion than the in-jet flow (see discussion in the Results section). This suggestion of more rapid corrosion environments being generated in off-jet positions is a strong recommendation for further testing to prove or disprove this possibility.

### 3.0 CORROSION THEORY

Corrosion as assessed by these studies can be accelerated by the relative movement between a corrosive fluid and a metal surface. This movement increases the transport of reactants to, and reaction products from, the reacting surface. Additionally, metal loss may be increased by physical damage to the metal surface or corrosion film when the fluid contains abrasive solid particles, or when cavitation or fluid droplet impingement occurs (two-phase flow).

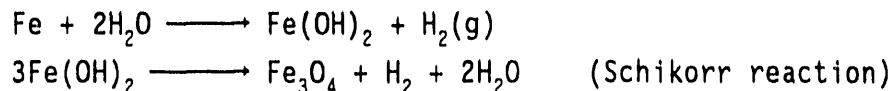
Erosion is defined as "the progressive loss of original material from a solid surface due to mechanical interaction between that surface and a fluid, a multi-component fluid, or impinging liquid or solid particles" (ASTM 1985). Erosion is often considered separately from the effects of corrosion. The fluids involved in this study, simulated NCAW and NCRW slurries, are corrosive to the subject carbon steel, but not significantly abrasive. Also, the fluid velocities involved generally are not high enough to cause erosion of the steel. This effect is expected with fluid velocities on the order of hundreds or thousands of feet per second.

Corrosion can be particularly rapid in areas of high turbulence where the fluid flow motion has a large component perpendicular to the surface (Cragolino, Czajkowski, and Shack 1988). Hence, geometry (the shapes of components in the system configuration that influence the fluid motion and impingement angle of the fluid) is extremely important when evaluating the effects of this type of corrosion. With all else equal, it is the fluid motion that controls the corrosion rate by transporting reaction products and dissolved film species away from the corroding surface and reactants to the surface. In this mode, fluid motion increases the corrosion rate of the material (Brubaker and Phipps 1979; Cragolino, Czajkowski, and Shack 1988).

The following sections discuss some of the theoretical background that will aid in understanding the corrosion processes involved with carbon steel in this investigation, particularly corrosion accelerated by a moving fluid.

### 3.1 CORROSION OF CARBON STEEL

Carbon steel corrodes in water environments when iron reacts with the water and dissolved oxygen to form oxidized iron species. The oxidized iron may stay in solution or precipitate in the form of iron oxides or hydroxides, depending on the solution chemistry, and form a film such as that shown in Figure 3.1. In deoxygenated systems the basic reactions are as follows:



for temperatures less than about 392°F (200°C) (Schikorr 1933). At higher temperatures, magnetite ( $\text{Fe}_3\text{O}_4$ ) forms directly. When the oxygen content of the system increases, gamma hematite ( $\gamma\text{Fe}_2\text{O}_3$ ), which is cubic and forms solid solutions with magnetite, may also form and become the dominant component of

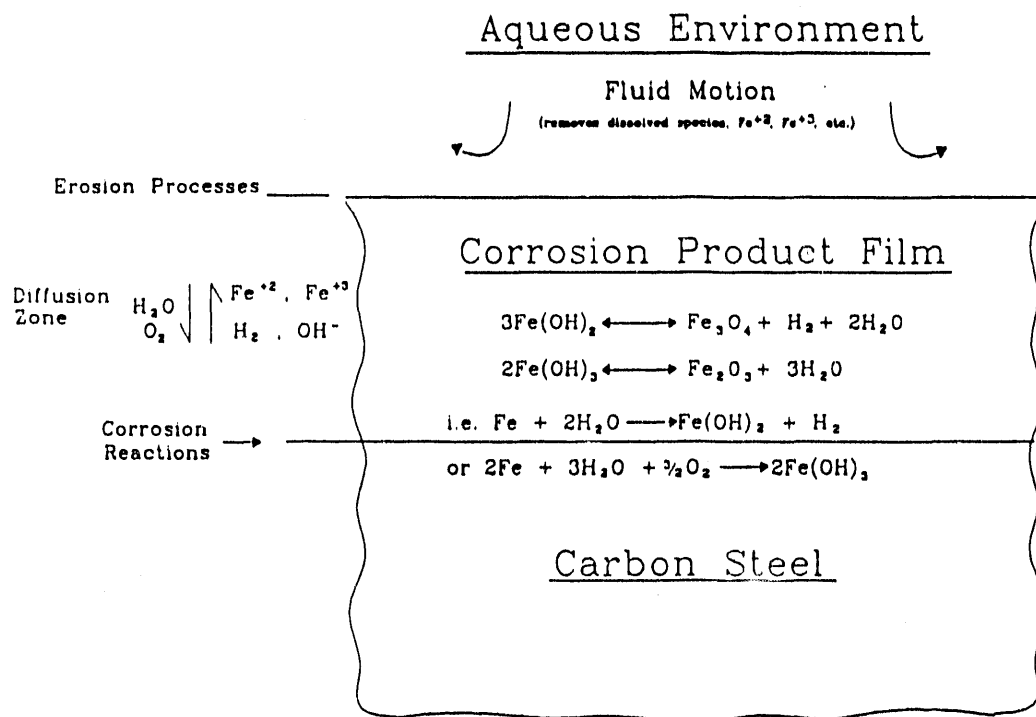
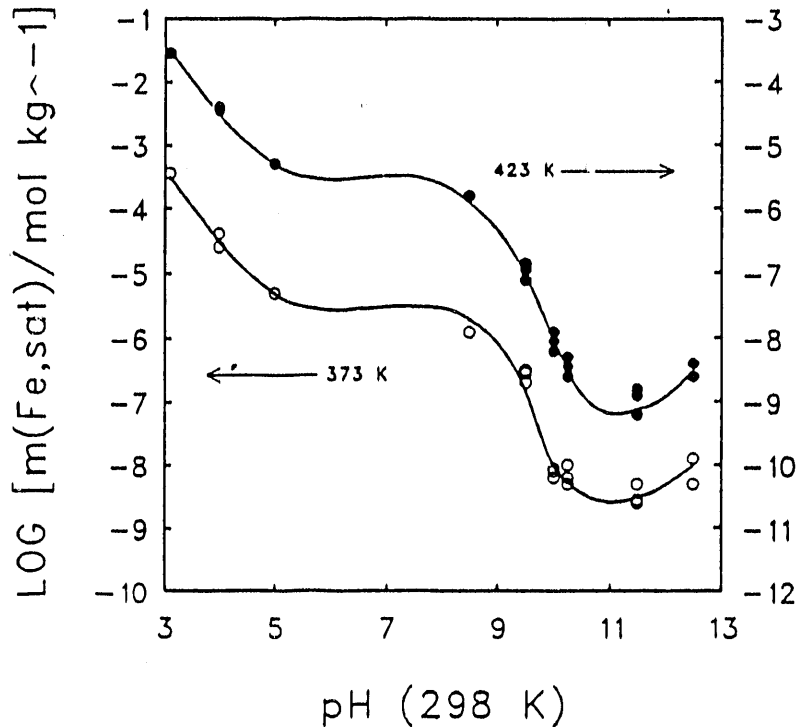


FIGURE 3.1. Model for Corrosion of Carbon Steel in High-Temperature Water Environment Showing Diffusing Species on Left Side of Illustration and Typical Reactions Forming a Film on Right Side

the corrosion film as the activity (concentration) of oxygen increases further. Under oxygenated conditions, additional hydroxyl ( $\text{OH}^-$ ) is formed instead of hydrogen gas.

Thermodynamic evaluations of the solubility of iron oxides and hydroxides in boiling water reactor systems indicate that ferric hydroxide controls the solubility of iron up to about  $300^\circ\text{F}$  ( $150^\circ\text{C}$ ) (Zarembo et al. 1986). At higher temperatures, iron solubility is controlled by magnetite. This creates a solubility maximum at about  $300^\circ\text{F}$  ( $150^\circ\text{C}$ ). The Zarembo et al. calculations also indicate that under deaerated conditions, ferrous hydroxide forms instead of ferric hydroxide. Higher hydroxyl concentrations significantly lower the solubility of the iron hydroxides (i.e., the "common ion effect"). The ferrous hydroxides consolidate to magnetite by the Schikorr reaction. The magnetite solubility is essentially unaffected by oxygen content over a range of 0.1 ppb to 1000 ppb. (These authors also point out that it is very difficult to get the oxygen content below ~10 ppb without elaborate procedures.) The magnetite has a solubility of about a factor of two greater than ferric hydroxide in the temperature range expected in the double-shell tanks (Zarembo 1986). An important point is that the oxygen content of the slurry, which is perhaps as low as 500 ppb in the test system, is not expected to have a large impact on the solubility of iron oxides in the expected double-shell tank environment.

The experimental results of Sanchez-Caldera, Griffith, and Rabinowicz (1988) agree with the above model, showing a distinct maximum at about  $300^\circ\text{F}$  ( $150^\circ\text{C}$ ) for corrosion in steam extraction lines with a solution pH range of 5 to 10 and oxygen concentration <200 ppb. Hence, the thermodynamic theory does appear to predict semi-quantitatively the behavior of carbon steel in hot water systems. Magnetite, believed to be a major component of the passivating film in the double-shell tanks (Divine et al. 1985), has a minimum solubility in the pH range 10 to 13, as shown in Figure 3.2 (Cragolino, Czajkowski, and Shack 1988). Though most of the studies referenced do not involve water solutions as concentrated as those in the double-shell tanks, they do indicate the behavior to be expected from the carbon steel. The carbon steel in the double-shell tanks is maintained at a very low corrosion rate (passivated



**FIGURE 3.2.** Experimental Solubilities of Magnetite at 423 and 373 K and 779  $\mu\text{mole/kg H}_2$  (Cragolino et al. 1988)

state) by keeping the tank contents at a very high pH, i.e., -13. Furthermore, Divine et al. state that dilution of the slurries like NCAW and NCRW with a corresponding decrease in pH may pose more of a corrosion problem than does the concentrated material now in the tanks (Divine et al. 1985).

The corrosion film formed on carbon steel by the reaction products controls the rate of further reaction by inhibiting the movement of reactants ( $\text{H}_2\text{O}$ ,  $\text{O}_2$ ) to the surface and reaction products ( $\text{Fe}^{2+}$ ) away from the surface. This inhibiting, or passivating, action is a function of the film properties such as thickness, porosity, and electrical resistivity. The film properties themselves are influenced by the corroding fluid motion, fluid chemistry, and system temperature. The fluid chemistry and temperature largely determine 1) the phases present in the corrosion film, 2) the texture and porosity of the film, and 3) the film solubility.

### 3.2 CORROSION MODELS

The corrosion of carbon steel in aqueous systems takes place as iron is oxidized to the +2 or +3 state, depending on the oxygen activity, and then goes into solution. When the concentration of the oxidized iron species, solution pH, temperature, and other aspects of the solution chemistry are suitable for precipitation of iron oxides, a passivating oxide film forms such as that illustrated by Figure 3.1. When this film is present, it will control the rate of carbon steel corrosion by controlling the rate at which reactants reach the metal surface and reaction products such as ferrous iron ( $\text{Fe}^{+2}$ ) leave the metal surface. The only time such a film will not be present is when the steel is cathodically protected (maintained at a negative potential greater than -0.44 V versus standard hydrogen electrode).

Standard corrosion reactions are accelerated by motion of the aqueous environment at the surface of the steel. This motion accelerates corrosion in several ways:

- steeper reactant and product concentration gradients are created across the passivating film
- the passivating film is thinned by causing it to dissolve faster
- portions of the film not tightly adhering to the surface may be dislodged and carried away.

Corrosion may be accelerated whenever fluid motion is present. However, fluid motion may or may not be important, depending on the magnitude of the effects of other processes.

The scientific and engineering literature addressing corrosion accelerated by fluid flow in aqueous systems can be separated by studies of the following systems:

- water systems without suspended solids at elevated temperatures and low levels of dissolved oxygen, i.e., boiler feedwater
- water systems with suspended solids (coal, limestone, silica, alumina, etc.) at ambient temperature and aerated or deaerated conditions

- two-phase liquid-gas systems consisting of vapor bubbles in a liquid or liquid droplets in a gas stream, i.e., some environments in steam extraction lines of power stations.

The two-phase systems will not be discussed here because this kind of system is not believed to be relevant to the DST environment.

Basically, the corrosion of carbon steel can be described in terms of the rate of mass loss per unit area as follows:

$$dm/dt = K (C - C_b) \quad (3.1)$$

where  $dm/dt$  = rate of mass loss per unit area  
 $K$  = the mass transfer coefficient  
 $C$  = the concentration of iron ( $Fe^{+2}$ ) at the solid-liquid interface  
 $C_b$  = the concentration of iron in the bulk liquid.

The mass transfer coefficient ( $K$ ) is an empirical function of the corrosion film thickness, porosity, ionic diffusion rates, and dissolution rate as well as the fluid velocity and angle of impingement. For many observations,  $K$  is found to be proportional to  $V^{0.9}$  ( $V \equiv$  velocity), and rate ( $dm/dt$ ) is proportional to  $K^n$  where  $n = 1$  to  $3$  (Cragolino, Czajkowski, and Shack 1988).

The mass transfer rate ( $dm/dt$ ) for corrosion is also a function of the concentration gradients of the reactants ( $H_2O$ ,  $O_2$ ) as well as reaction products ( $H_2$ ,  $OH^-$ ,  $Fe^{+2}$ ,  $Fe^{+3}$ ) (see Figure 3.1). In most cases the critical concentration gradient is that of the oxidized iron species (i.e.,  $C - C_b$  divided by a diffusion distance). The magnitude of the concentration gradient is a function of the equilibrium solubilities of the iron oxides and the rate at which they form as well as the diffusion distance. These concentrations are in turn a function of temperature, water chemistry (e.g., pH) and the electrical potential of the metal surface.

Complexing ions for iron, such as chloride or sulfate, promote corrosion by increasing the solubility of iron and contributing to the degradation of any passivating film on the iron. The complexing agent increases the stable concentration of iron in solution, increasing the diffusion flux of iron away from the surface because of the larger effective concentration gradient. The

higher solubility of iron may lead to the breakdown of the passivating film, further increasing the corrosion rate.

Finally, the characteristics of the film of corrosion products influence the corrosion rate. The porosity of the film is one such variable that is believed to be a controlling factor and is included specifically in the corrosion model of Sanchez-Caldera:

$$dm/dt = K \Theta (C - C_p) \text{ (simplified form)} \quad (3.2)$$

where  $\Theta$  is the porosity of the oxide film. The porosity of the film determines the percentage of the metal surface that is in direct contact with the corroding fluid.

Corrosion influenced by fluid flow depends on a complex combination of physical, chemical, and geometric characteristics (i.e., the fluid flow patterns and velocity of a jet impinging on a sample surface; see discussion in Section 6.0) of the system in which it occurs. Because of the many complex variables involved, it is best to determine the rates of corrosion for a given system with tests that accurately simulate the actual conditions under which the corrosion is expected to occur.

### 3.3 FLOW PATTERNS IN IMPINGING ROUND JETS

The jet pumps to be used in the double-shell tanks are assumed to generate round jets. These jets can be characterized as axisymmetric and having either laminar or turbulent flow. The Reynolds number ( $Re = UDd/\mu$ ) determines if the jet will be turbulent or laminar, where  $U$  (cm/s) is the average fluid velocity at the nozzle,  $D$  (cm) is the nozzle diameter,  $d$  (g/cc) is the density, and  $\mu$  (g/cm-s) is the viscosity. A Reynolds number above about 10,000 indicates turbulent flow, and below a few thousand laminar flow. Flows with intermediate Reynolds numbers may fluctuate between laminar and turbulent. The jet in the double-shell tanks definitely will be turbulent:

$UDd/\mu = 656250$  for  $U = 1750$  cm/s,  $D = 15$  cm,  $d = 1.25$  g/cc, and  $\mu = 0.05$  g/cm-s. The three velocities used in the NCAW test were 11, 24, and 46 ft/s and with  $D = 0.635$  cm, the corresponding Reynolds numbers are 5238,

11430, and 21907. If the viscosity is actually less by a factor of two, as it might be, all of the test jets should also have been turbulent.

When a round jet impinges on a flat surface, the vertical fluid motion is redirected into a radial wall jet moving parallel to the wall surface. As shown in Figure 3.3, the impinging jet consists of three regions: the free

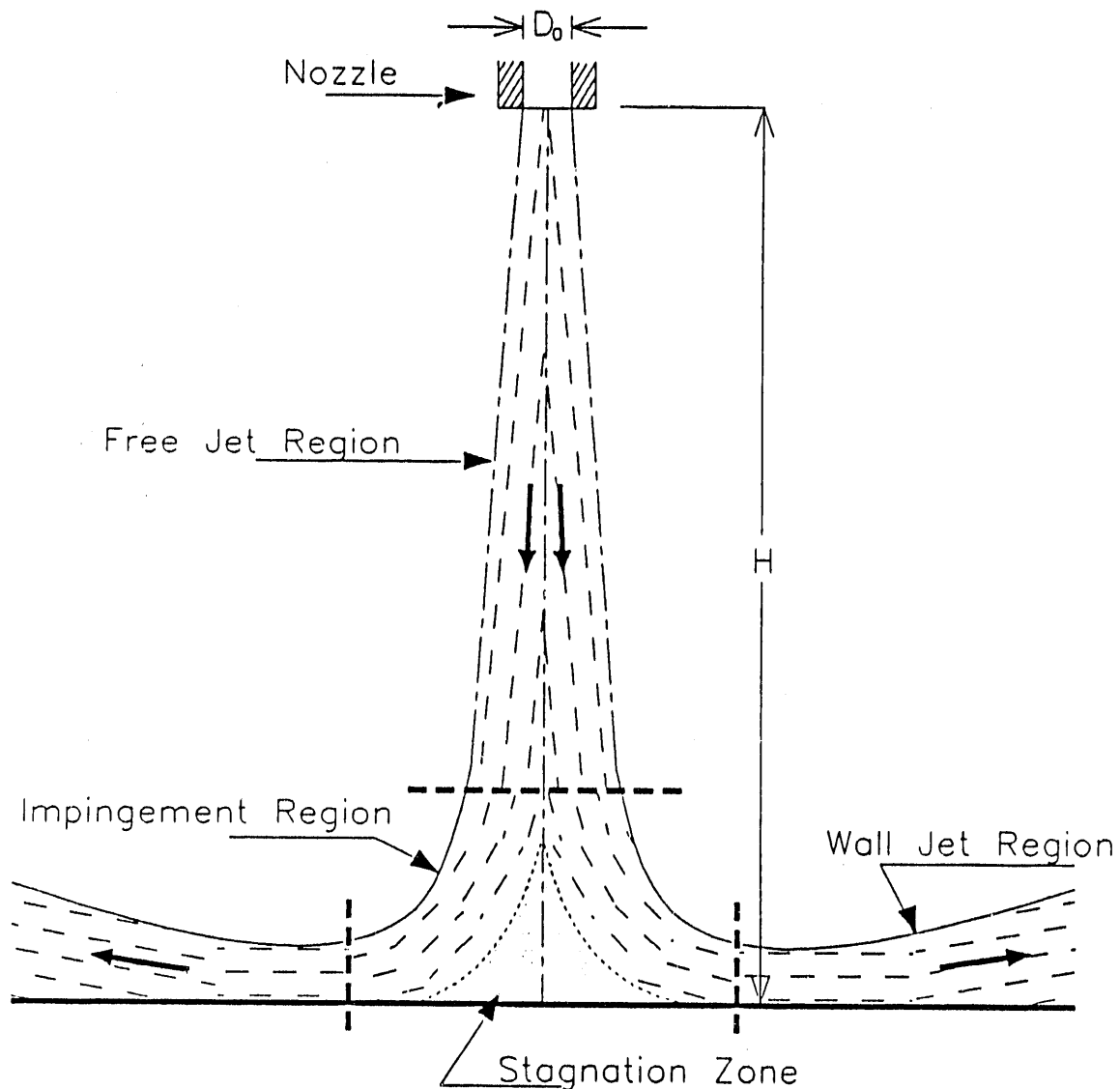


**FIGURE 3.3.** Impinging Fluid Jet Showing Flow Characterized by Three Principal Regions: 1) Free Jet Region, 2) Impingement Region, and 3) Wall Jet Region

jet, the impingement region, and the wall jet. A number of papers and books (e.g., Tani and Komatsu, 1966; Beltaos and Rajaratnam, 1974; Rajaratnam, 1976; Giralt, Chia, and Trass, 1977) describe the hydrodynamics of the impinging circular jet, giving the pressure profile, the centerline velocity of the jet as it approaches the wall, the radial velocity of the fluid as a function of position measured from the centerline of the jet, shear stress as a function of radial position, etc.

In general, these jets have a centerline stagnation point on the surface that coincides with the point of maximum hydrostatic over pressure. The fluid velocity parallel to the impingement surface and shear stress on that surface increases linearly from zero with the radial distance from the centerline reaching a maximum at about  $r/H = 0.14$ , where  $r$  is the radial distance from the centerline of the jet and  $H$  is the distance from the jet nozzle to the impingement surface, or about 0.2 inches for the NCRW test and 0.7 inches for the NCAW test. The edge of the impingement zone for the NCRW test is about 0.4 inches from the centerline, and about 1.1 inches from the centerline for the NCAW test. (Note that the fluid in a turbulent jet is not motionless at the centerline stagnation point on the impingement surface; just the average velocity is zero.) Hence, the NCRW test coupons included the impingement zone and an appreciable area that was contacted by the wall jet. The NCAW test coupons resided entirely within the impingement zone.

Chia, Giralt, and Trass (1977) have shown that for the impingement region, the local mass transfer coefficient is proportional to the square root of the jet nozzle velocity. Hence, in this region, it is expected that if the corrosion rate is controlled by the transport of corrosion product species away from the surface of the coupon, the corrosion rate should be proportional to the square root of the jet nozzle velocity--i.e.,  $K$  in equation (3.1) is proportional to the square root of the nozzle velocity. If the flow conditions are such that the corrosion rate is controlled by the thickness of an essentially static boundary layer (laminar sub-layer; see Schlichting, p. 604), then  $K$  in equation (3.1) is expected to be inversely proportional to that thickness (i.e.,  $K \propto D/\delta$  where  $D$  is the diffusion coefficient of the critical species and  $\delta$  is the boundary layer thickness). The  $\delta$ , as defined,

is inversely proportional to the square root of the shear stress at the wall. Since shear stress is proportional to the square of the velocity,  $K$  will be proportional to velocity, and corrosion processes controlled by the laminar sub-layer thickness will show a rate proportional to velocity. These are two possible jet velocity dependencies that might be shown by the NCRW/NCAW tests.

#### 4.0 TEST APPROACH

During the retrieval of the contents of the DSTs, the interior surface of the carbon steel walls and floors will be subjected to impinging jets of slurry as a result of the action of the pumps used to suspend the settled solids. As already discussed in Section 3.0, the many factors affecting corrosion of carbon steel make it difficult to predict corrosion rates for a specific set of conditions. Therefore, to obtain corrosion data, tests have been conducted using a system that accurately reproduces the actual or predicted conditions.

The method selected for assessing the effect of an impinging jet on the corrosion rate of tank steel was to approximate the geometry, temperature, and chemistry of the waste tanks, and then choose the parameters that will be modified by the pumping action for further testing. Of those parameters (e.g., slurry jet impingement velocity, angle of slurry jet impingement, duration of jet impingement), impingement velocity was selected for the initial scoping tests with NCRW simulant, and impingement velocity and duration of impingement velocity were selected for the tests with NCAW simulant. The differences between the two tests required modifications to the test apparatus so that the NCAW test could be conducted at a higher temperature and the impingement time could be varied. This is described in more detail in Sections 4.2 and 4.3. These modifications produced a test condition that was believed to be an even more accurate simulation of the DST environment during retrieval operations. The methods also demonstrated the importance of impingement velocity in NCRW and NCAW slurry systems.

For these tests, the simulated, nonradioactive slurry composition was matched to the expected composition of the waste slurry. Carbon steel of a composition similar to that used to fabricate the waste tanks was used for the test coupons. The temperature and velocity of slurry striking the test coupons matched that expected to occur in the tanks during retrieval. Weight losses were measured at intervals throughout the test without removing the oxide layers from the surface of the coupons. This type of cyclic exposure was necessary since the limited number of coupons that could be accommodated

in the test equipment did not permit recovery of individual, intermediate coupons at each interval. Some effect from the cyclic exposure and from rinsing and drying the coupons removed to estimate the weight loss is likely, but the magnitude of this effect is unknown. Final, time-averaged corrosion rates were determined at the completion of the tests after chemically stripping the remaining oxide from the surfaces of the coupons.

As stated previously, the objective of the tests was to determine if DST slurry motion will increase the corrosion rate of DST steel, and if so, how the rate will change as a function of velocity. However, these tests were not suitably designed to determine exact, long-term corrosion rates for the actual waste tanks (see Section 5.1.2 for a more complete discussion of this point) since the data from the samples as tested give the time-averaged corrosion rates. These time-averaged corrosion rates are good approximations to the long-term corrosion rates if there is a cycling of the corrosion rate because of spalling of the corrosion films. If cyclic spalling does not occur, then the time-averaged corrosion rates asymptotically approach the long-term corrosion rates with increasing time. In this case, the time-averaged corrosion rates are greater than the expected long-term corrosion rates. In either case, the tests provide a good indication of the effects of the variables being tested.

Other types of tests have been used to evaluate corrosion accelerated by moving fluids, particularly for flow in pipelines. One example, a spinning disk technique, has been used to evaluate different materials under similar conditions in a single test. This method has been used to evaluate abrasion and corrosion in simulated flow conditions (the test article spins in the fluid, rather than the fluid flowing past the test article). It is not known how well this method would predict results for an impinging jet of slurry. In addition, measuring the effects of impingement versus nonimpingement cycling is not readily adaptable to this method. Some work has been done to correlate the results of different types of corrosion tests involving fluid flow, but the work has not shown conclusively that the spinning disk method would provide accurate information about accelerated corrosion caused by an impinging

jet of slurry. Therefore, the method selected for this test is believed to better correlate the test results with anticipated conditions during waste retrieval operations.

#### 4.1 TEST APPARATUS

As described above, the test apparatus used for the NCAW and NCRW tests was essentially the same, consisting of a slurry tank, recirculating pump, piping with suitable nozzles for the jets, and holders for positioning the coupons. When it was decided to include impingement time along with impingement velocity, the apparatus was modified to include a switching mechanism capable of varying the total time that the slurry jets impinged on the coupons. The sections below describe the test apparatus in greater detail.

##### 4.1.1 NCRW Test Apparatus

The test apparatus for the tests with simulated NCRW slurry, shown in Figure 4.1, was designed to expose disks of DST carbon steel to jets of slurry at an elevated temperature over the range of velocities expected in the tanks

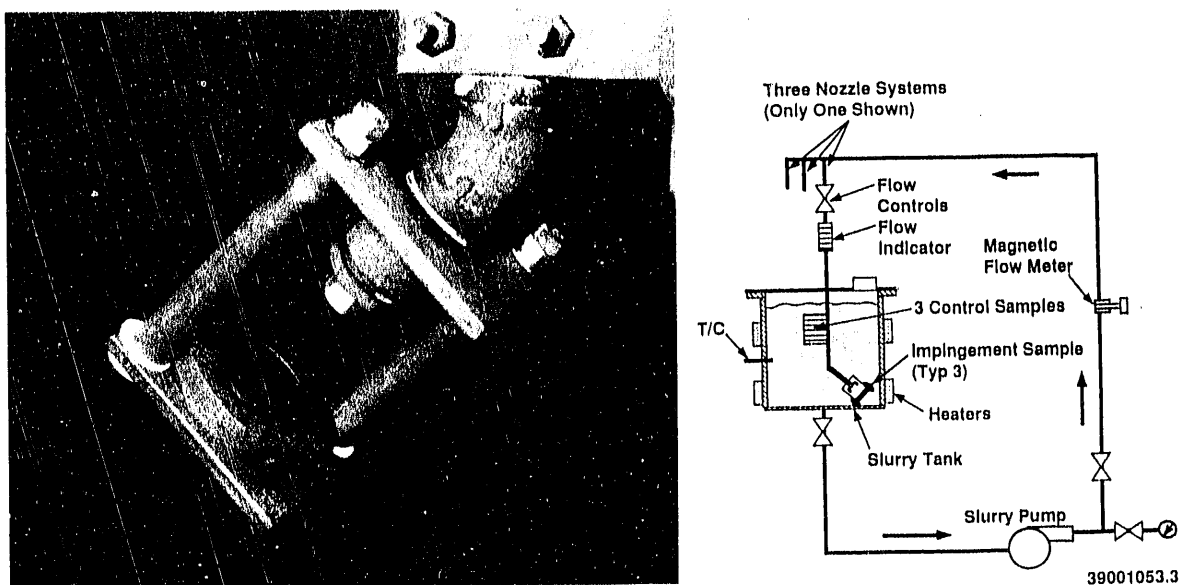


FIGURE 4.1. Nozzle and Impingement Coupon, and Illustration of Test Apparatus Used for the NCRW Jet Impingement Corrosion Test

during waste retrieval. The tank was made of carbon steel and was large enough to hold about 40 gallons of slurry simulant. Three test positions were located near the bottom of the tank pointing away from each other at a 120° angle. The device that held the test coupons consisted of brackets that were hard mounted so the test coupons could be placed at a fixed distance (1.5 in.) in front of three 0.26-in-dia slurry jet nozzles. The disk-shaped coupons (1.5 in. dia) were held in the brackets by set screws and positioned so that the disks were oriented perpendicularly to the jet and so the jet impinged the center of each disk.

In addition to the disk specimens, another set of specimens (control coupons) was included in a sample holder designed to provide a non-flowing but otherwise similar environment to the disk specimens. These coupons were used to measure the quiescent corrosion also occurring on the impingement coupons. The reason for this treatment is described in detail in subsequent sections.

As indicated by Figure 4.1, the jet nozzles and all of the specimens were immersed in the slurry contained in the test tank. A centrifugal pump with a dual gland mechanical seal drew slurry from the bottom of the tank and circulated it back into the tank through the jet nozzles. A flow meter on each slurry line monitored the volumetric flow rate to each of the nozzles. The target volumetric flow meter readings were determined by the diameter of the jet nozzle orifice and the desired jet velocity. The flow rates were controlled separately for each line via manual control valves in each line. The slurry circulation also served to keep the sludge-like solids in suspension within the test tank.

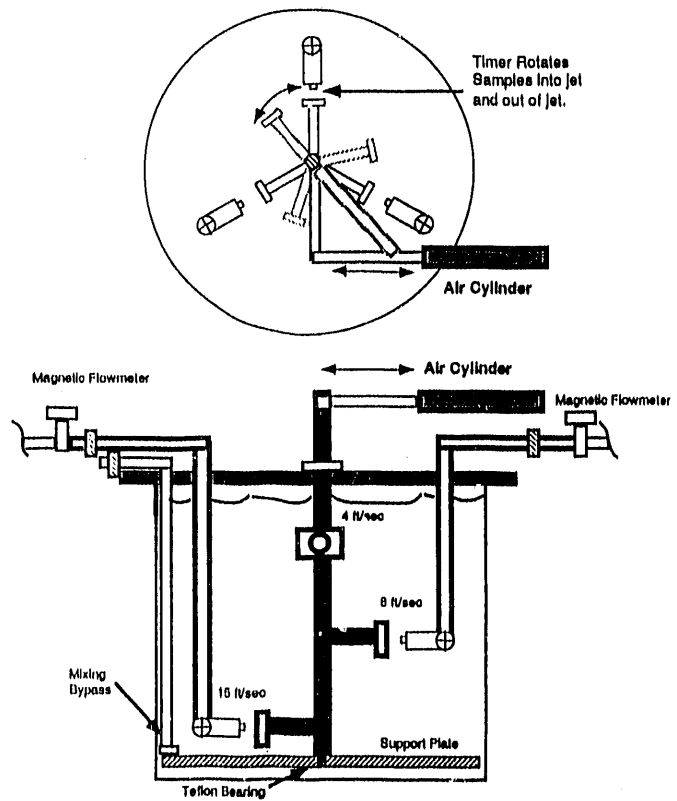
A lid on the tank reduced evaporation of water from the slurry. Some evaporation losses were still observed while conducting the NCRW test at 180°F (82°C). Additional losses were observed through a leaky pump seal. These losses were offset by additions of deionized water and, sometimes, a caustic solution to maintain the volume and high pH of the slurry.

#### 4.1.2 NCAW Test Apparatus

The test apparatus used for the NCAW tests was similar to that used for the NCRW tests. The principal differences between the tests were the size of

the test coupons; the slurry jet impingement velocities; the movement of the NCAW samples in and out of the jet stream; the distance from the slurry jet nozzle orifice to the sample surface; the vapor-tight lid on the tank, which permitted a higher test temperature (214°F to 217°F); and a different slurry composition. The coupon holders were also submerged in the slurry as shown in Figure 4.2: a total of six impingement coupons, two for each test velocity at three different levels in the tank. The three levels were necessary to minimize exposure of the impingement coupons to flow from more than one jet.

The disk holder was rotated by a pneumatic cylinder on a cycle timer to bring one coupon of each of the three pairs into the flow for a preset interval (see Section 4.3.3). This technique permitted two different jet impingement times for each slurry velocity.



NCAW Erosion Corrosion Test

FIGURE 4.2. Test Apparatus Used for NCAW Jet Impingement Corrosion Test

The distance from the nozzle orifice to the disk surface was 5 in. and was also controlled with a special alignment tool within approximately 0.1 in. The distance between each nozzle and impingement coupon was originally selected to provide a relatively flat velocity profile, based on a "free jet" model, across the face of the coupon. A sensitivity analysis was performed using the free jet model to determine the allowable jet misalignment value. In the analysis, anticipated jet velocities were calculated as a function of radial position from the centerline of the jet. Corrosion rates, assuming a velocity dependence, were then calculated for various jet velocities. The analysis indicated that a jet misalignment of  $\sim 1/8$  in. would result in less than a 5% error, which was considered to have negligible effect on the test results. Further analysis showed that the "free jet" model does not accurately model the impingement region of an axially symmetric circular jet (see Beltaos and Rajaratnam 1974). However, because of the symmetry of the circular jet and resulting radial velocity distribution, the original conclusion regarding jet misalignment is probably still valid.

The disks were held in place by three set screws tipped with Teflon to prevent physical scarring of the specimen and to provide electrical insulation for preventing galvanic coupling of the specimen and holder. As before, stainless steel (17-4 pH stainless steel) gland nuts were selected for the nozzles in the test system. A special tool was fabricated to check the alignment of each of the impingement coupons with the nozzles. The NCAW impingement coupons, the alignment tool, and control coupons are shown in Figure 4.3. The larger NCRW impingement coupons are also shown for comparison. One end of the tool was machined to fit tightly into the nozzles; the other end aligned with the proper position of the coupons. Corrosion or wear of the nozzles was determined to be insignificant over the course of the test, since no change was noted in the close fit of the alignment tool with the inside diameter of the nozzles.

The tightly fitting lid used for the NCAW test prevented liquid from evaporating. The slurry was maintained at a temperature near its boiling point (214°F to 217°F) by a heating blanket surrounding the slurry tank. The

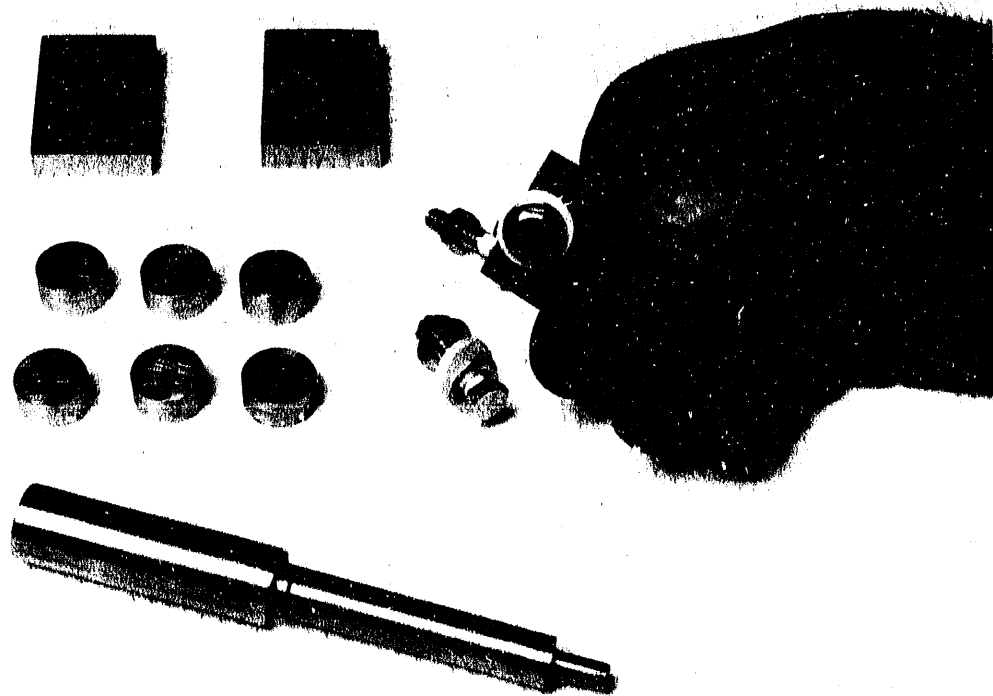
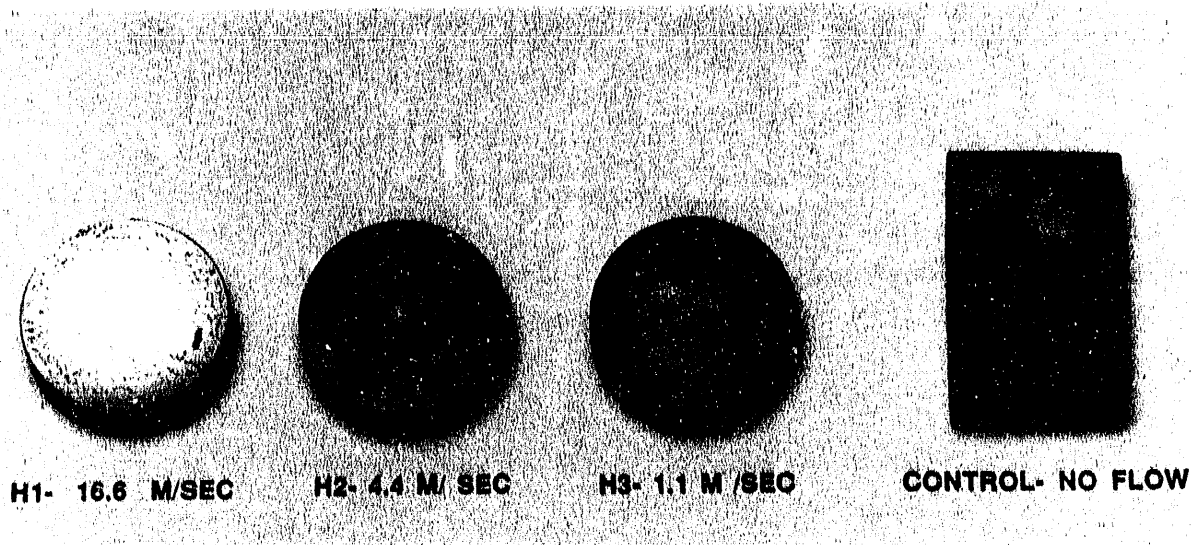


FIGURE 4.3. ASTM A-537 Carbon Steel Coupons Used for the NCRW Corrosion Test (Top) and the NCAW Test (Bottom). Note the device used to check alignment of the NCAW impingement coupons after installation in the test apparatus.

system was pressurized slightly (~5 in. water) during testing to permit operation at the higher temperature without boiling the slurry, thus minimizing cavitation in the recirculating pump.

## 4.2 TEST MATERIALS

The laboratory investigations used actual steel materials and simulated slurries for the test materials to assess the effects of DST waste slurry corrosion on the carbon steel used to fabricate the DSTs. Coupons used in this work were fabricated from archived samples of carbon steel used in the construction of some of the DSTs, and the simulated waste slurries chemically and physically (slurry abrasivity and vol% solids) resembled the actual wastes. This section describes simulated NCRW and NCAW slurries and the test coupons used in the corrosion testing.

### 4.2.1 Simulated NCRW Slurry

Table 4.1 lists the composition of the simulated NCRW slurry used for the corrosion experiment. The slurry was composed primarily of zirconium-based solids, with considerable amounts of carbonate and halides, particularly fluorides. This simulant is similar to the NCAW slurry in terms of its suspended solids and pH. However, because of the lack of iron in the NCRW slurry and the presence of chloride and fluoride, which can complex with iron to produce

TABLE 4.1. Composition of Simulated NCRW and Simulated NCAW Slurries

<u>Component</u>	<u>Simulated NCRW Slurry</u>		<u>Simulated NCAW Slurry</u>	
	<u>Supernate Concentration, mmol/g</u>	<u>Solids Concentration, mmol/g</u>	<u>Supernate Concentration, mmol/g</u>	<u>Solids Concentration, mmol/g</u>
Al			0.19	2.81
Cr			0.006	0.047
Fe			0.0001	1.15
K			0.103	<0.001
Na	2.10	4.26	3.89	7.92
Zr		1.27		
F	0.78	3.95	0.10	
NO <sub>3</sub>	0.60	0.40	2.05	
SO <sub>4</sub>			0.16	
pH <sup>4</sup>	13		13	
Sp.gr. (g/ml)	1.25		1.24	

soluble iron species, the NCRW slurry might be expected to be more corrosive to the carbon steel than NCAW slurry.

#### 4.2.2 Simulated NCAW Slurry

WHC prepared and supplied the simulated NCAW slurry used for the corrosion test in March of 1989. PNL received approximately 70 gallons of simulated NCAW for the test. The simulated slurry was prepared before analysis of the 101-AZ core samples was complete, so the slurry composition was not based on results of the core sample analysis. Instead, the procedure used to produce the simulant closely resembled the major steps that occur during the generation of actual NCAW, including creation of an acidic (primarily nitrate) solution, sugar denitration of the acidic waste, and subsequent caustic neutralization. Table 4.1 lists the chemical composition of the simulated NCAW slurry.

The pH of the as-received slurry was ~13, consistent with the Hanford tank farm specification for liquid waste storage (pH>12). At intervals throughout the test the pH was measured and found to be stable, so periodic adjustments with caustic were not necessary.

#### 4.2.3 Carbon Steel Test Coupons (NCRW and NCAW Tests)

The test coupons for both corrosion tests were fabricated from a piece of archived DST carbon steel (ID: H-1470) supplied by WHC. The coupons exposed to the slurry jets, called "impingement coupons," were disk shaped (1.5-in. dia by 0.375-in. thick) for the NCRW test. The coupons for the NCAW test were smaller (0.75-in. dia by 0.375-in. thick) so they could be exposed to a uniform impingement velocity across their surfaces (see Section 4.1.2). Based on a free-jet model and the NCRW test configuration, a large velocity gradient would have existed across the surface of the larger NCRW coupons [see page 5-20, Chemical Engineers Handbook, Perry, Chilton, and Kirkpatrick (1963)]. However, the authors believe that the differences between the slurry impingement patterns for the two tests were not so well described by the free-jet model (see Section 3.3), and that the differences in the effects of the flow patterns between the tests were possibly not so different for the case of direct impingement.

Three rectangular, nonimpingement control coupons were included in both the NCRW and NCAW tests to measure "quiescent" corrosion rates in each simulant in each test. These coupons were 2 in. x 1.3 in x 0.375 in., drilled with 0.3-in. holes for hanging. Figure 4.3 shows the coupons used in both tests. Table 4.2 gives the weights and dimensions for all of the test coupons at the beginning of the NCRW and NCAW corrosion tests.

Near the completion of the NCAW test, we learned that the sample of steel provided for the test had been archived from the "AP" tank farm, not from the "AZ" tank farm as originally thought. A-537 carbon steel was used to fabricate the AP tanks, while ASTM A-515 grade 60 steel was used to fabricate the AZ tanks. The chemical composition of A-515 steel varies slightly from the composition of A-537 steel. A sample of the test material was chemically

TABLE 4.2. Pretest Weights and Dimensions for the NCRW and NCAW Corrosion Test Coupons

Sample	Weight, g	Shape	Dimensions, in.
<u>NCRW</u>			
H1	84.5439	disk	1.498 x 0.374
H2	84.6451	disk	1.497 x 0.375
H3	84.7920	disk	1.498 x 0.375
HC1	117.3469	rectangular	1.975 x 1.277 x 0.378 <sup>(a)</sup>
HC2	120.3804	rectangular	1.977 x 1.294 x 0.038 <sup>(a)</sup>
HC3	123.2461	rectangular	1.970 x 1.330 x 0.380 <sup>(a)</sup>
<u>NCAW</u>			
H1	20.9875	disk	0.750 x 0.375
H2	21.0753	disk	0.750 x 0.377
H3	21.1075	disk	0.750 x 0.376
H4	20.9874	disk	0.749 x 0.376
H5	20.9467	disk	0.750 x 0.375
H6	21.0867	disk	0.750 x 0.377
H7	121.3404	rectangular	1.975 x 1.341 x 0.376 <sup>(b)</sup>
H8	121.2907	rectangular	1.966 x 1.344 x 0.376 <sup>(b)</sup>
H9	122.0228	rectangular	1.988 x 1.337 x 0.376 <sup>(b)</sup>

(a) Each coupon was drilled to provide a 0.257-in.-dia hole for hanging.

(b) Each coupon was drilled to provide 0.316-, 0.316-, and 0.315-in.-dia holes, respectively, for hanging.

analyzed to verify its composition. Table 4.3 lists the composition of the WHC sample, compared with the ASTM specifications for grade A-537 and A-515 grade 60 carbon steel plate. This comparison verifies that the composition of the archived sample falls within the limits of the specification for A-537. The difference in corrosion resistance of A-515 and A-537 carbon steel in the simulated test slurry is not known, but it is anticipated to be negligible based on a comparison of the static corrosion rates of these general kinds of steels in simulated, typical Hanford-type wastes from previous tests (Divine et al. 1985).

#### 4.3 CORROSION TEST PARAMETERS

The two most important test parameters and controls for the corrosion tests were to 1) maintain the slurry jet impact velocities at predetermined values, and 2) maintain the bulk slurry temperature at a constant setpoint. A third test parameter was established for the NCAW test: to cycle the coupons in and out of the path of the jets to vary jet incidence times on the coupons, a procedure that was not followed in the preceding NCRW test. The bases for these test parameters and details of these conditions are described below.

TABLE 4.3. Comparison of Chemical Compositions for A-515 Steel, ASTM A-537 Carbon Steel, and Erosion-Corrosion Test Material

Material	Composition, wt%									
	Fe	C	Mn	Si	P	S	Cr	Ni	Mo	Cu
A-515 <sup>(a)</sup> grade 60	Bal.	0.24 (max)	0.98 (max)	0.13 to 0.45	0.035 (max)	0.04 (max)	--	--	--	--
A-537 <sup>(b)</sup>	Bal.	0.24 (max)	0.65 to 1.40	0.13 to 0.55	0.035 (max)	0.04 (max)	0.25 (max)	0.25 (max)	0.08 (max)	0.35 (max)
H-1470 <sup>(c)</sup>	Bal.	0.20	1.31	0.30	0.013	0.006	0.19	0.12	0.01	0.05

(a) Type of steel used to construct tanks in the AZ tank farm.

(b) Type of steel used to construct tanks in the AP tank farm.

(c) Identification number for steel used in this test.

#### 4.3.1 Jet Velocities

The basis for the slurry jet velocities for the NCAW test was the assumption of a two-pump arrangement for the mixer pumps in 101-AZ (with a standoff distance of the pump from the tank wall of ~15.5 ft), and an exit velocity of slurry from the pump based on a nozzle discharge parameter of  $U_0 D = 29.4$  ft<sup>2</sup>/s. Three slurry jet velocities were investigated during the NCAW test. Velocities were chosen to represent a range of probable conditions in the actual waste tank during retrieval operations. A high velocity of 15 ft/s (4.6 m/s) was selected to approximately match the maximum velocity of the slurry impinging on the tank wall. A low slurry velocity of 4 ft/s (1.2 m/s) and an intermediate velocity of 8 ft/s (2.4 m/s) were also tested to provide a range of conditions to more accurately determine the response of the corrosion process to jet velocity. These jet impact velocities (high, medium, and low) were achieved by pumping the slurry through three 0.26-in.-dia (0.66-cm-dia) nozzles at volumetric flow rates of ~7.5, 4, and 2 gallons/min  $\pm 5\%$  (28.4, 15.1, and 7.6 L/min), respectively, at standoff distances (nozzle to specimen) of 5 in.  $\pm 0.1$  in. (12.7 cm). These free jet model velocities correspond to nozzle exit velocities of ~46, 24, and 11 ft/s, respectively.

The jet velocities chosen for the NCRW tests spanned a larger range than those for the NCAW tests. The first two NCRW jet velocities, 3.6 ft/s (1.1 m/s) and 14.4 ft/s (4.4 m/s), corresponded closely to the first and third NCAW test velocities, 4 ft/s (1.2 m/s) and 15 ft/s (4.6 m/s), thus providing a good basis for comparing the two test series. The third test jet velocity was that expected at the mixer pump nozzle opening, 54.5 ft/s (16.6 m/s) (i.e., the highest slurry velocity that will occur in the DST during retrieval operations), thus extending the velocity range considerably beyond that used for the NCAW test.

#### 4.3.2 Temperature

A normal temperature of the waste in the DSTs is reported to be as high as ~140°F (60°C), but the power expended by the mixer pumps during sludge resuspension could cause the slurry temperature to increase to as much as ~217°F (103°C) during retrieval. Since the test tank would not seal well during the NCRW test, a lower temperature of 180°F (82°C) was used to keep water

evaporation rates from becoming excessive during the test. The test tank closure was redesigned so that the test system could be sealed and slightly pressurized (~5 ft of water). This improvement permitted the NCAW test to be run at 214 to 217°F (101 to 103°C), thus matching the expected retrieval temperature without the water loss problem. Pressurization with compressed air minimized cavitation in the pump that could otherwise have been a problem with the slurry at or near its boiling point.

#### 4.3.3 Impingement Times

During waste retrieval operations, the mixer pump assemblies will rotate about their vertical axes in an oscillating motion while the pumps direct the slurry jets at the settled solids. A result of this pump assembly rotation is that the jets will strike a particular point on the tank floor or wall in a cyclic manner about 10% of the total pump operating time, with an approximate cycle time of 5 minutes. The cyclic impact was simulated in the NCAW test by adding switching equipment to the test apparatus. The switching mechanism moved the coupons and their holders into and out of the flows of the fixed jets on a repeating cycle of 0.5 minute in one position and 4.5 minutes in the switched position. In this manner, one set of coupons was impinged by the jets for 0.5 minute out of every 5 minutes, simulating the in-tank conditions. The second set of coupons was impinged for 4.5 minutes of each 5-minute cycle. Although the longer exposure period for the second set of coupons does not match expected retrieval conditions, it was included to investigate the effect of jet impact cycle time on the corrosion rate of the steel. The earlier NCRW test did not include a mechanism for switching the coupons, so the exposure time for the coupons was 100% in the flow of the jets.

#### 4.3.4 Air Sparge

In addition to the three parameters for the NCAW test (jet velocity, slurry temperature, and impingement time), original plans called for introducing air into the NCAW test system to simulate the action of airlift circulators in the DST. Airlift circulators are suspended in the fluid of some of the aging waste tanks to provide some mixing and cooling of the waste slurry. It is probable that these circulators will continue to operate during sludge mobilization and during a portion of waste retrieval. Bubbling air into the

waste would be expected to keep the dissolved oxygen concentration near its solubility limit and to introduce carbon dioxide into the slurry, both of which were thought to influence the corrosion rate of the carbon steel. The conditions produced by the airlift circulators were simulated in the NCAW corrosion test using an air sparge tube in the test tank to continuously bubble air into the slurry. The target rate for air flow was scaled to approximate the volumetric flow of the airlift circulators operating in the tank, and was set to ~0.011 cfm (0.3 L/min). Soon after the test began the sparge line plugged. At the first scheduled examination of the test coupons the plugged line was cleared, but it plugged again soon after the test was restarted. Numerous attempts were made to keep the air sparge flowing, but plugging with precipitated salts continued to be a problem. Eventually, use of the air sparge was discontinued in the NCAW test.

The effect from shutting off the air sparge was estimated. Limited data on oxygen solubility for this type of solution complicated the analysis, but estimates have shown that the concentration of oxygen in the slurry could decrease to perhaps parts per million by reacting with iron in the closed test system at the rate observed on the control specimens. (In the test system the slurry was periodically exposed to air when the tank was opened to retrieve the specimens for interim weight loss measurements, thereby replenishing some of the dissolved oxygen in the slurry.) However, as discussed in Section 3.0, the corrosion rate of carbon steel is expected to be quite insensitive to oxygen concentration down to concentrations as low as 0.1 ppb, far below those anticipated during testing. Based on this analysis, we concluded that a significant effect on corrosion rate from decreasing oxygen concentration with time was not expected over the planned operation of the NCAW test.

Similar estimates of the effects of carbon dioxide on corrosion in the system were made. Because of the high concentration of free hydroxide in the slurry, CO<sub>2</sub> absorption from the air sparge would not be sufficiently reduce the concentration of caustic in the slurry and thereby influence the corrosion rate. Thus, a significant effect on corrosion of the NCAW test coupons was not anticipated from discontinuing the air sparge.

#### 4.4 TEST PROCEDURES

This section describes the procedures followed for both tests, including preparation of the coupons, conduct of the test, and final cleaning and examination of the coupons.

##### 4.4.1 Coupon Preparation

The disk-shaped impingement coupons and rectangular control coupons were machined from a heat-treated, archived sample of DST carbon steel to make the test surfaces coplanar with the original steel plate surface. Before the tests, all coupons received uniform surface finishes with 240 grit silicon carbide sandpaper to remove any corrosion products and provide a known starting point for each coupon. The coupons were then washed, rinsed in acetone, and dried to remove any residual contaminants that might have been present from handling the specimens.

Prior to installation in the test system, each specimen was carefully weighed and measured (see Table 4.2 for weights and dimensional measurements).

##### 4.4.2 Test Protocol

For each test, about 40 gallons of slurry simulant was added to the test tank. The test specimens were fixed in position in their holders, and the apparatus was submerged in the slurry simulant. The lid was bolted in place. The pump was started and the slurry passed through the nozzles and impinged on the corrosion samples. At that time (for the NCAW test), the sample switching mechanism that moved the samples into and out of the center of the slurry jets was activated. The slurry tank heater was turned on, and when the temperature of the slurry reached within 10°F of the setpoint temperature the test was considered to have started. Initial heating of the tank usually required 4 to 5 hours starting from room temperature, and about 1 hour after intermediate inspections when the slurries did not cool significantly. While the tests were running, the temperature, flow rates through each of the three nozzles, and switching frequency (for the NCAW test) were periodically monitored by the operator. The operator recorded the operating data, including data associated with any adjustments to the slurry flow rate and the temperature.

The power to the heaters and the pump was shut off periodically so the samples could be evaluated. The tests were considered stopped at that time. When the slurry had cooled sufficiently to remove the samples (usually less than 1 hour), the lid was removed and the coupons were taken out of the slurry. The specimens were removed from their holders, rinsed in tap water, and examined as described in the next section. Following the examination, the samples were reinstalled in the test apparatus. Water was added to the tank to make up for evaporative loss if the slurry level had dropped by more than about 1/2 in. The pH of the slurry was measured every 1 to 2 weeks throughout the tests, particularly if the slurry level had to be adjusted. Caustic was used to keep the pH at or above 13. The adjustments were needed primarily during the NCRW test because of the faulty pump seal. The tests were restarted in essentially the same sequence used for initial startup.

At the end of the test period, the slurries were drained out of the tank and the system was rinsed to remove any residual slurry. The flowmeter calibration was checked by pumping water through the system (i.e., the amount of water pumped in a given time interval was compared to that indicated by the flowmeter).

#### 4.4.3 Coupon Cleaning and Examination

For interim evaluations, the coupons were well rinsed in deionized water and dried (~1 hour at 125°C for the NCRW test, and 30 minutes at ~110°C for the NCAW test). They were then allowed to cool to ambient temperature in a desiccator. Each of the coupons was carefully weighed to within  $\pm 0.1$  mg. An optical survey of the coupons at 30X was also made at this time to screen them for any major changes in the corrosion film. The coupons were photographed to document their appearances at each of the interim periods.

Following completion of the test, final as-tested weights were determined as described above with the oxide surface films (corrosion products) intact. The coupons were then chemically cleaned by immersing them in inhibited hydrochloric acid. Each coupon was repeatedly cleaned at 2- to 3-minute immersion cycles, then dried and weighed until its weight loss per cleaning cycle was equivalent to the weight loss per cleaning cycle indicated by a separate reference coupon of uncorroded carbon steel. The weight loss rate of

the impinged coupons during the chemical cleaning process dropped to that exhibited by the blank coupon over the same time interval needed for the weight loss rate of the control coupon to drop to the rate for the blank coupon. It appears that the thicker film on the exposed face of the impinged coupon was cleaned off in the same time as the thin film on the control coupons. The weight change from cleaning for the impinged coupons was corrected by assuming the nonimpinged areas incurred the same weight loss per unit area as the control coupons. We conclude that these film weight determinations are probably as accurate as indicated by the reproducibility of the control coupon film weight determination, ~4%.

Both before and after chemical cleaning, the NCAW coupons were examined by scanning electron microscopy (SEM) to show the general condition of the corrosion product layer on the coupon surface and how it differed from stagnant conditions to the slurry impingement conditions, and from low to high slurry velocity conditions. Energy dispersive x-ray analyses were also employed to examine the substrate metal and the corrosion product layer. The interim and final results of the NCAW test coupon examinations are presented in Section 5.0. Similar extensive SEM examinations of the NCRW coupons were not performed for the earlier NCRW test.

## 5.0 TEST RESULTS

Results of the corrosion testing were collected in two phases, intermediate and final. Intermediate weight losses were determined at different intervals throughout the test without disturbing the oxide surfaces on the samples, other than to rinse the samples with water, dry them, and weigh them. The NCRW test inspections were conducted at 1, 7, 14, 27, 40, 55, 68, 81, 94, and 107 days from the start of the test. The NCAW test inspections were conducted at 7, 16, 30, 42, 51, 92, 120, and 150 days. Results from these interim measurements were used to determine when the baseline (control) corrosion and impingement corrosion weight change rates reached a presumed steady-state condition. These measurements were also used to calculate presumed steady-state corrosion rates, assuming that the mass of the corrosion film did not change.

Determination of the final results involved removing the oxide films from the test coupons by inhibited chemical cleaning, then measuring total metal losses to develop calculations of final time-averaged baseline corrosion and impingement corrosion rates. SEM examination was performed on the NCAW specimens after completion of the test, both before and after oxide film removal.

### 5.1 EXPECTED RESULTS

This section discusses the results that were expected from these tests. Interim test results and final test results are discussed in Sections 5.2 and 5.3, respectively. The discussion of expected results is based on information from the open literature. Section 5.1.1 describes mechanical (i.e., "erosion") processes. Section 5.1.2 describes processes that are dominated by chemical corrosion as the cause of material loss.

#### 5.1.1 Mechanical (Erosion) Processes Causing Material Loss

Erosion is defined by ASTM as "the progressive loss of original material from a solid surface due to mechanical interaction between that surface and a fluid, a multi-component fluid, or impinging liquid or solid particles." The ASTM definition of erosion does not include chemical interactions of the surface with the fluid, or "corrosion." Corrosion responses involving a flowing fluid are more difficult to predict or to classify as typical because the

effects of corrosion can vary so widely. If the corrosion phenomenon for a given fluid is strictly "uniform" corrosion, with no localized corrosion, the weight loss response may look similar to erosion weight loss response, although neither the magnitude of weight losses nor the time scales involved would necessarily be expected to be similar.

#### 5.1.2 Chemical "Corrosion" Dominant Processes

If chemical corrosion dominates in these systems, as it probably does because of the low abrasiveness of these slurries (Miller number of ~8 for NCAW and effectively 0 for NCRW) and the relatively low slurry jet velocities, then the weight change observed is the sum of the loss of metal by corrosion and the gain of corrosion film on the surface of the test coupon. Under these conditions the weight changes observed may be positive or negative, depending on 1) the physical and chemical character of the corrosion film, 2) the proportion of the weight loss due to metal corrosion, and 3) weight gain from film formation. All of these quantities can be expected to change with time. The result is that the observed weight changes could mimic expected erosion behavior without erosion being a factor at all. The intermediate weight change observations do not differentiate between the various potential combinations of weight gain and weight loss. Therefore, to calculate corrosion rates from observed weight changes, one must make assumptions about the components that can contribute to the weight changes. One such assumption would be that the weight of the oxide film is not changing when the observed coupon weight changes become constant from measurement to measurement (i.e., the weight change is determinant, and therefore the weight change indicates the corrosion rate).

The amount of corrosion that  $\delta W$  metal has incurred on a material coupon is determined from the difference between the initial coupon weight and the final coupon weight (i.e., the coupon is free of corrosion products). During corrosion the specimen will change weight at a rate according to the equation:

$$\delta W(\text{meas.})/\delta t = \delta W(\text{metal})/\delta t + \delta W(\text{film})/\delta t$$

or

$$\delta W(\text{metal})/\delta t = \delta W(\text{meas.})/\delta t - \delta W(\text{film})/\delta t$$

(5.1)

where  $\delta W(\text{metal})/\delta t$  = the weight of metal lost per unit area  
 $\delta W(\text{meas.})/\delta t$  = the observed weight change per unit area, and  
 $\delta W(\text{film})/\delta t$  = the weight change of corrosion film per unit area;  
 all during the increment of time ( $\delta t$ ).

From Equation 5.1, it is clear that at any particular time, the specimen weight change rate,  $\delta W(\text{meas.})/\delta t$ , is the sum of two numbers: the rate at which metal is converted into corrosion products,  $\delta W(\text{metal})/\delta t$ , and the rate at which corrosion products form film on the specimen surface,  $\delta W(\text{film})/\delta t$ . Therefore, the actual corrosion rate cannot be determined from only a weight change rate observation unless the rate of weight change in film adhering to the specimen is known to be negligible or unchanging between observations.

Figure 5.1 illustrates how  $\delta W(\text{meas.})/\delta t$  (see Equation 5.1) might be observed as a function of time (intermediate weight change) in a corrosion experiment or test. In the figure, it is assumed that the oxide film forms at some arbitrary rate,  $\delta W(\text{film})/\delta t$ , that is initially rapid but decreases with time, asymptotically approaching zero in time (only one of many possibilities is shown as a dashed line). Also shown in the figure are two different corrosion rate trends,  $\delta W(\text{metal})/\delta t$ , that one might observe (shown as solid lines). Adding the film-forming rate term,  $\delta W(\text{film})/\delta t$ , to the corrosion rate term,  $\delta W(\text{metal})/\delta t$ , gives the observed weight change term,  $\delta W(\text{meas.})/\delta t$  (shown as a dot-dash line). As shown, two quite different  $\delta W(\text{meas.})/\delta t$  curves result. However, when (or if) the  $\delta W(\text{film})/\delta t$  term becomes small, then the  $\delta W(\text{meas.})/\delta t$  approaches the actual corrosion rate,  $\delta W(\text{metal})/\delta t$  (i.e.,  $\delta W(\text{meas.})/\delta t = \delta W(\text{metal})/\delta t$ ). The change rate term for film weight can be a large component of the  $\delta W(\text{meas.})/\delta t$  value, causing it to be a very misleading indicator of corrosion rate unless the film-forming characteristics of the system are well known and can be taken into account.

Uniform corrosion rates on coupons are typically determined by running a series of identical coupons under identical conditions for different lengths

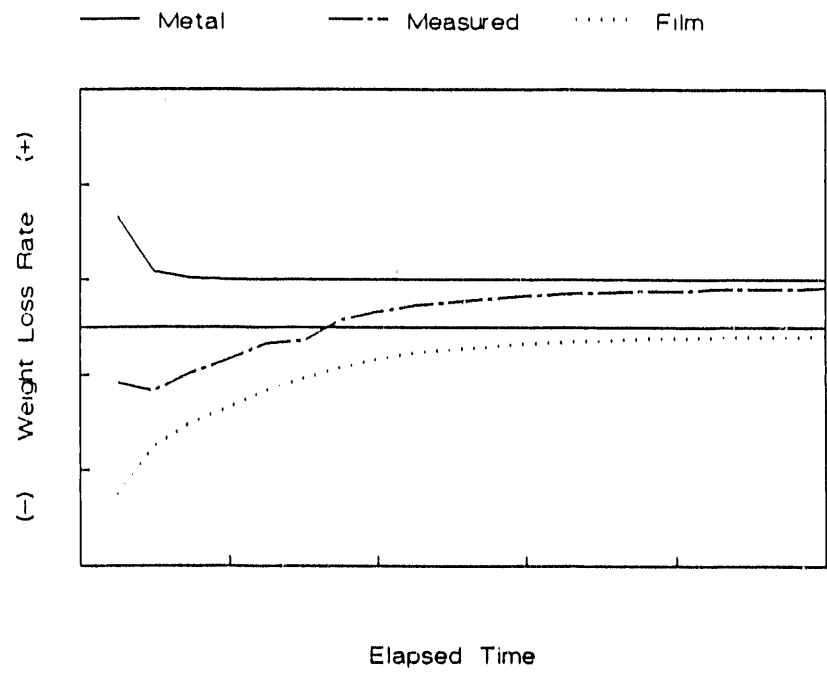
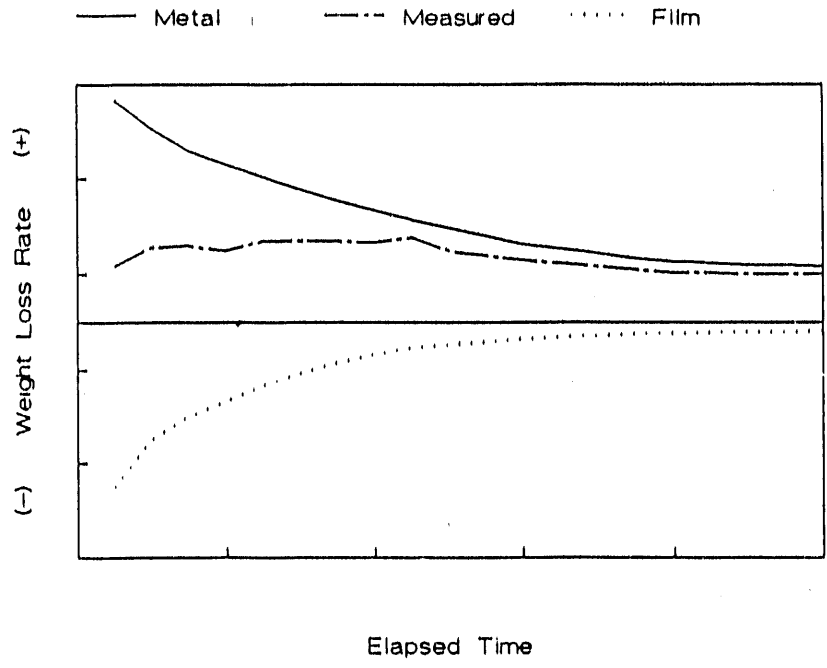


FIGURE 5.1. Two Examples of Hypothetical Weight Change Rate Versus Time Dependencies for Steel Corrosion Observations. Note that a negative weight loss rate is really a weight gain rate.

of time. These coupons are chemically cleaned and the actual metal loss per unit area for that time interval determined. When subsequent metal loss rates are the same, then a steady-state corrosion rate has been determined (Fontana and Greene 1978). The reason for this procedure is related to Equation 5.1. Initially, the corrosion rate will change with time as a corrosion film develops on the surface, causing the corrosion reaction to slow down. At some point the corrosion film dissolves at the same rate that new film forms. When this happens, a steady-state corrosion process is established and the rate of metal loss per unit area does not change with time. Only actual determinations of metal loss with time unequivocally indicate the rate of metal loss, eliminating the possibility that changes in the oxide film-forming rate are counterbalancing changes in the metal loss rate, giving a "false" steady-state.

The NCAW and NCRW slurry corrosion tests were designed to compare the behavior of waste tank carbon steel under a series of slurry jet impingement velocities. The design of these tests did not permit absolute determination of the final steady-state corrosion rate because only one specimen was run under a given set of conditions. However, a time-averaged corrosion rate was determined for each condition from the total metal lost during the experiment. Assuming that each coupon will exhibit the same corrosion behavior with time (e.g., Figure 5.1), the time-averaged rate should indicate the effect of different corrosion conditions (i.e., different slurry jet impingement times and velocities) on the carbon steel. Therefore, the time-averaged corrosion rates provide a good basis for concluding that these variables do influence the corrosion rate. More tests need to be run using the multiple specimen protocol per test condition if definitive, final steady-state rates are to be determined.

The final corrosion rates occurring in these tests can be calculated if one assumes that when the measured weight change per unit area per unit time becomes constant, steady-state conditions have been established and measured weight changes are equivalent to metal loss (i.e., the weight of the corrosion film per unit area remains constant). This is a reasonable assumption for determining a long-term corrosion rate, but the value is only as reliable as

the assumption. Another assumption is that the corrosion film structure is stable, and it will not begin spalling off the metal surface. If the film began spalling periodically, then the time-averaged corrosion rates determined by these tests may be closer to the actual long-term rates than is the above estimate. Also, one is assuming that pitting corrosion is not taking place, which would not show up as a significant weight change. Subsequent evaluation of the test coupons did not reveal any pitting.

## 5.2 INTERIM TEST RESULTS

Periodically throughout the corrosion tests, interim weight loss measurements were made on each of the rectangular control coupons and the circular impingement coupons. Section 4.3 describes the procedure used for taking interim measurements.

Because there was only one coupon for each condition, the corroded surfaces had to remain intact for the entire test. Cleaning the oxide from the coupons at each interval to determine accurate weight losses would have invalidated the results by reintroducing the coupons into the hot corrosive slurry without the protection of the passivating oxide films. Since the interim measurements did not involve removal of the oxide surface layers, the weight loss responses are not an exact indication of the amount of specimen corrosion. However, the measurements adequately reflect the trend in weight change so we can infer the shape of the weight loss curve, and thereby estimate if and when the results appear to reach an equilibrium condition. After an initial period of high weight loss rates from the impingement coupons, weight losses from the samples appeared to level off at lower values, indicating the system had reached an apparent equilibrium state that would be more useful for predicting responses to long-term exposures to corrosion conditions. Other inferences from the shape of the curves must be made cautiously for reasons discussed in Section 5.1.

The weight losses from the control coupons measured at each interval were also used as a means of evaluating the weight losses from the impingement coupons by separating the weight losses resulting from quiescent corrosion only

from weight losses resulting from corrosion of the faces exposed to the jets. This process is illustrated later. Interim weight measurements for the test coupons are given in the Appendix.

### 5.2.1 Control Coupons

Table 5.1 lists the weight changes per unit area for the control coupons at each of the interim inspections. These coupons represent three replicate coupons exposed to the same conditions in the test tank. Averages of the pre-cleaning weight loss results for the three control coupons were used to adjust the pre-cleaning weight loss measurements recorded for the impingement specimens to distinguish baseline corrosion weight loss from impingement corrosion weight loss (see Section 5.2.2).

Initial negative weight loss values for the NCAW coupons mean that a corrosion product layer formed and accumulated on the initially clean specimens at a faster rate than the metal and/or film was removed by the solution.

**TABLE 5.1.** Cumulative Weight Loss as a Function of Time for the NCRW and NCAW Control Coupons

NCRW Coupon	Cumulative Weight Loss Per Unit Area, mg/cm <sup>2</sup> (a)(b)										Final(c)
	Inspection Interval (days from start of test)										
	1	7	14	27	40	55	68	81	94	107	
HC1	0.000 (.00)	0.020 (.02)	0.104 (.08)	0.165 (.07)	0.109 (-.06)	-0.219 (-.11)	-0.217 (.00)	-0.272 (-.05)	-0.276 (-.01)	-0.328 (-.05)	1.650
HC2	0.006 (.01)	0.020 (.01)	0.089 (.07)	0.165 (.08)	0.135 (-.03)	-0.085 (-.05)	-0.095 (-.01)	-0.201 (-.10)	-0.215 (-.01)	-0.222 (-.01)	1.751
HC3	0.002 (.00)	0.051 (.05)	0.098 (.05)	0.154 (.10)	0.088 (-.06)	-0.138 (-.05)	-0.127 (.01)	-0.185 (-.06)	-0.203 (-.01)	-0.224 (-.02)	1.712
Avg.	0.003	0.030	0.097	0.161	0.111	-0.148	-0.146	-0.219	-0.231	-0.258	1.704
NCAW Coupon	7	16	30	42	51	92	122	150	Final		
H7	-0.050 (-.05)	0.004 (.05)	0.089 (.09)	0.199 (.11)	0.317 (.12)	0.633 (.31)	0.917 (.29)	1.20 (.28)	2.58		
H8	-0.045 (-.05)	-0.006 (.04)	0.078 (.07)	0.176 (.10)	0.302 (.12)	0.638 (.34)	0.934 (.29)	1.19 (.26)	2.52		
H9	-0.037 (-.04)	0.014 (.05)	0.081 (.07)	0.166 (.09)	0.257 (.09)	0.627 (.37)	0.868 (.24)	1.10 (.23)	2.37		
Avg.	-0.044	0.004	0.083	0.180	0.292	0.633	0.906	1.16	2.49		

- (a) Negative weight loss values (weight gain) indicate accumulation of a corrosion product layer.  
 (b) Values in parentheses (mg/cm<sup>2</sup>) indicate the measured change during the time between measurements.  
 (c) The final weight loss was determined after removal of the oxide film by chemical cleaning (see Section 4.4.3).

Eventually, the rate of film formation was reduced by the increasing thickness of the oxide, until an apparent equilibrium was reached where the reaction of the base metal to form the corrosion products is approximately equal to the rate of film removal. The NCRW control coupons showed almost the opposite response, first showing weight losses followed by weight gains (see Table 5.1). This is discussed further in Section 6.1.

Figure 5.2 shows typical surface areas of the NCAW control coupons after completion of the test and before the oxide surface was chemically removed. The pictures, taken at 250X by a scanning electron microscope, show a thin oxide layer on the surfaces. The oxide layers closely reproduce the original sample surface texture that was formed by grinding the specimens as part of the sample preparation procedure. The original finish marks are still very sharp, indicating little erosion of the surface. This also indicates that the corrosion mechanism involved between carbon steel and the simulated NCAW slurry is apparently a uniform mechanism, with no evidence of pitting or cracking of the substrate. This was again confirmed when the coupons were chemically cleaned. Observation of the NCRW control coupons at a low magnification suggested that uniform corrosion had occurred on those coupons as well.

#### 5.2.2 Impingement Coupons

Weight loss from the impingement coupons involves a combination of impingement corrosion and baseline corrosion mechanisms acting on different surface areas of the coupons. In the test tank the slurry jet impinges on one circular face of each coupon, resulting in a weight loss specific to that area of the exposed face. It is the corrosion rate associated with the exposed face impingement area that would correspond to wall thinning in the DSTs. The remaining surface area of each impingement coupon is exposed to the bulk solution, but under much reduced flow conditions. Therefore, it was assumed that the carbon steel on these surfaces, the side and back face of each coupon, would react with the solution at a rate equivalent to the control coupons. The weight losses attributed to corrosion of the front faces are determined by adjusting the total weight loss by a ratio of the impinged front face area to the rest of the sample surface area using the baseline corrosion rate derived

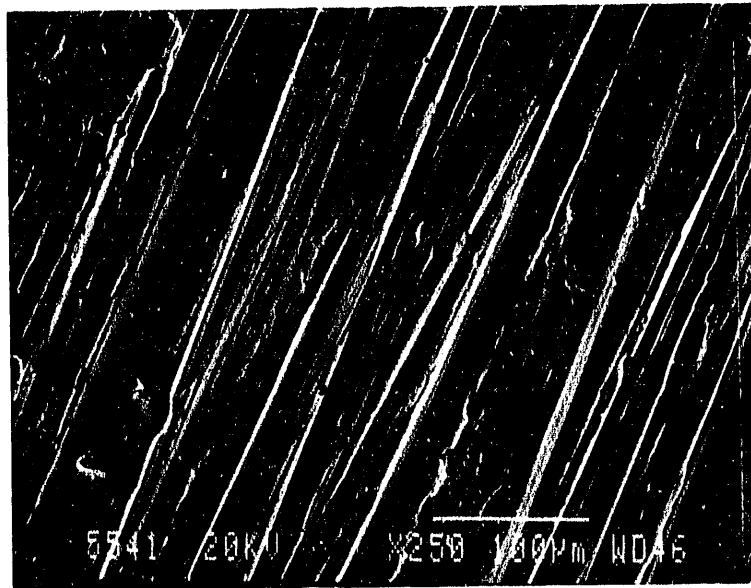
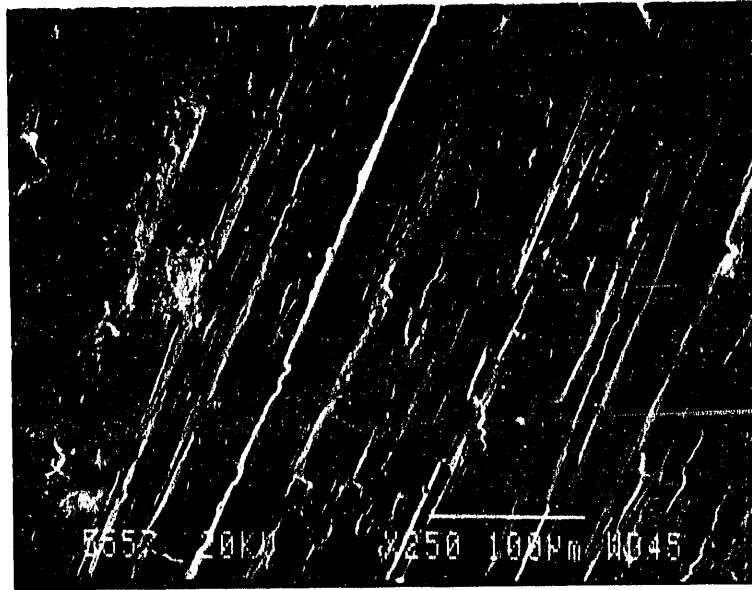
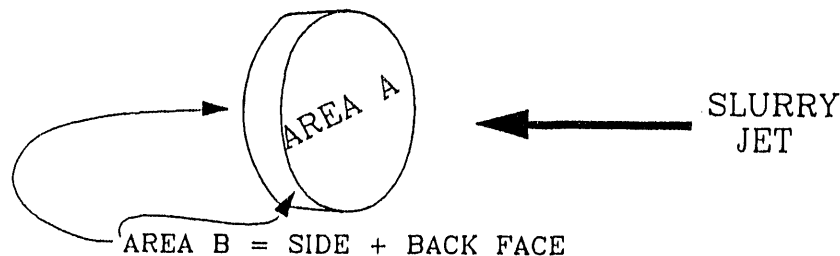


FIGURE 5.2. Typical Areas of the Surfaces of Two NCAW Control Specimens Before Oxide Removal (250X). Marks visible from initial sample preparation show only slight uniform corrosion. Exposed 150 days in simulated NCAW at  $\sim 217^{\circ}\text{F}$ .

from the rectangular coupons. Figure 5.3 illustrates this method of determining the impingement corrosion weight loss.

Table 5.2 shows the tabulated results of the adjusted weight loss calculations before and after removal of the oxide surface films, adjusted as described above for the impingement coupons at each of the inspection intervals. This information was also used during the test to determine if the weight loss rates had reached steady-state. For the NCAW test coupons, the initial weight loss rates were erratic and low, rose to a maximum, and were then followed by long-term weight losses at lower rates (see Figure 6.3). For the NCRW test coupons, the initial weight loss rates were scattered and changed erratically with time. The NCRW weight loss rates approached similar values in time, but were still erratic near the end of the test (see Figure 6.3).



TO CALCULATE EROSION-CORROSION RATE:

- Determine average control coupon weight loss/cm<sup>2</sup> (g/cm<sup>2</sup><sub>CONTROL</sub>) for same time (T)
- Multiply (g/cm<sup>2</sup><sub>CONTROL</sub>) by AREA B of the impingement coupon to get weight loss due to corrosion of side and back face = g<sub>AREA B</sub>
- Subtract g<sub>AREA B</sub> from total weight loss to obtain weight loss for AREA A (g<sub>AREA A</sub>), the impingement face of the coupon

$$\text{Erosion-Corrosion Rate} = (KxW)/(AxTxD) = \text{mils per year (mpy)}$$

- where
- K = Constant (3.45 x 10<sup>6</sup>)
  - W = Weight Loss (G<sub>AREA A</sub>), g
  - A = AREA A Surface Area, cm<sup>2</sup>
  - T = Time, h
  - D = Density of Carbon Steel (7.88 g/cm<sup>3</sup>)

FIGURE 5.3. Impingement Coupon and Method Used to Calculate "Adjusted" Corrosion Rate

**TABLE 5.2.** Comparison of Adjusted Cumulative Weight Loss as a Function of Time for the NCRW and NCAW Impingement Coupons

NCRW Coupon <sup>(b)</sup>	Cumulative Adjusted Weight Loss per Unit Area, mg/cm <sup>2(a)</sup>										
	Inspection Interval (days from start of test)										
	1	7	14	27	40	55	68	81	94	107	Final <sup>(c)</sup>
H1	0.417 (.42)	1.954 (1.53)	3.491 (1.54)	9.835 (5.35)	13.11 (3.27)	15.84 (2.73)	16.69 (0.85)	18.99 (2.30)	21.27 (2.28)	23.78 (2.51)	23.14
H2	0.083 (.08)	0.996 (.92)	1.769 (.77)	4.168 (2.60)	7.070 (2.90)	9.947 (2.88)	11.63 (1.68)	13.81 (2.18)	15.27 (1.46)	16.69 (1.42)	16.29
H3	0.056 (.06)	0.195 (.14)	0.333 (.14)	0.829 (.50)	1.415 (.59)	3.136 (1.72)	3.705 (.57)	5.214 (1.50)	7.621 (2.41)	9.030 (1.41)	8.971
NCAW Coupon <sup>(d)</sup>	7	16	30	42	51	92	122	150	Final <sup>(c)</sup>		
H1	0.19 (.19)	1.11 (.93)	2.35 (1.23)	3.85 (1.50)	5.12 (1.27)	7.36 (2.24)	9.14 (1.78)	10.40 (1.26)	17.80		
H2	0.22 (.22)	1.08 (.87)	2.38 (1.29)	3.39 (1.01)	3.65 (.26)	4.13 (.48)	4.68 (.55)	4.96 (.26)	9.70		
H3	0.40 (.04)	1.64 (1.25)	3.01 (1.36)	4.48 (1.47)	5.75 (1.27)	7.82 (2.07)	10.40 (2.58)	12.00 (1.60)	20.01		
H4	0.29 (.29)	1.11 (.84)	1.86 (.75)	3.08 (1.22)	4.05 (.97)	6.79 (2.74)	7.62 (.83)	8.20 (.58)	14.19		
H5	0.33 (.33)	1.81 (1.48)	4.07 (2.26)	4.07 (1.32)	5.39 (1.45)	6.84 (4.21)	11.40 (3.36)	15.10 (1.66)	23.16		
H6	-0.69 <sup>(e)</sup> (-.69)	0.90 (1.59)	2.98 (2.08)	5.14 (2.16)	6.70 (1.56)	12.90 (6.20)	16.80 (3.90)	20.30 (4.50)	33.14		

(a) Values in parentheses (mg/cm<sup>2</sup>) indicate the measured weight change during the time between measurements.

(b) Velocity (ft/s): H1 = 54.5; H2 = 14.4; H3 = 3.6.

(c) Final weight losses similar to Table 5.1 values, except these include the adjustment for removal of equivalent weight from nonimpingement surfaces.

(d) Velocity (ft/s): H1 = 4; H2 = 4; H3 = 8; H4 = 8; H5 = 15; H6 = 15. Impingement Time (min/5-min cycle): H1 = 4.5; H2 = 0.5; H3 = 4.5; H4 = 0.5; H5 = 4.5; H6 = 0.5.

(e) Negative weight loss values (weight gain) indicate accumulation of a corrosion product layer.

Photomicrographs of the surfaces of the NCAW impingement coupons were taken after the test was completed but before the oxide layers were removed. The SEM examination provided information about the surface conditions after exposure to the test conditions. The photomicrographs provided information on the texture and structural integrity of the corrosion film and how these properties were affected by changes to the test parameters. Figures 5.4, 5.5, and 5.6 show 1000X, 1000X, and 500X magnification views, respectively, of representative areas on the surfaces of the impingement coupons exposed to the low-velocity, mid-velocity, and high-velocity jets. The surfaces shown in these photomicrographs are of the oxide layer on the coupons before final cleaning.

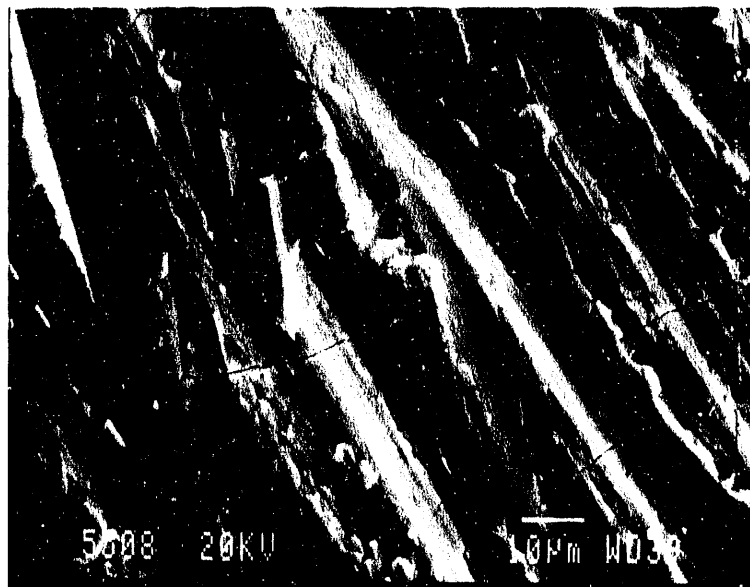
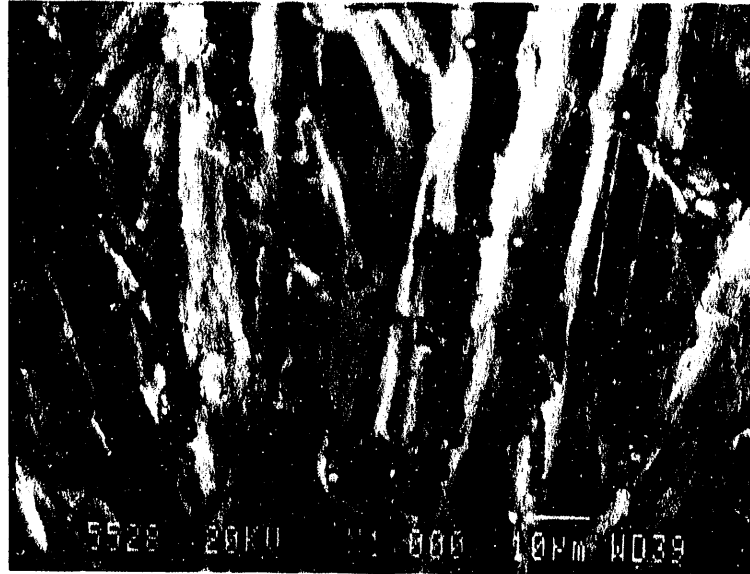


FIGURE 5.4. NCAW Impingement Coupons Exposed to Low-Velocity Jets (4 ft/s) Before Oxide Removal (1000X). Top photo is of coupon H2 (0.5 min/cycle) and bottom photo is of coupon H1 (4.5 min/cycle).

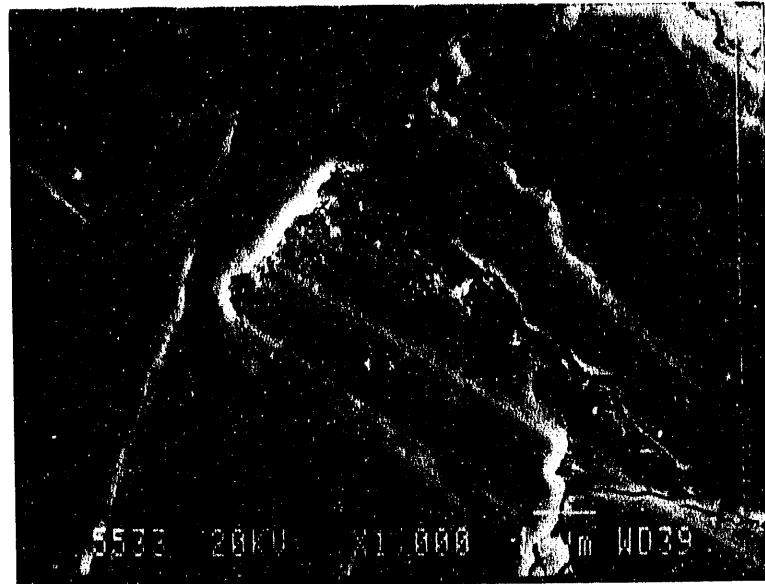


FIGURE 5.5. NCAW Impingement Coupons Exposed to Medium-Velocity Jets (8 ft/s) Before Oxide Removal (1000X). Top photo is of coupon H4 (0.5 min/cycle) and bottom photo is of coupon H3 (4.5 min/cycle).

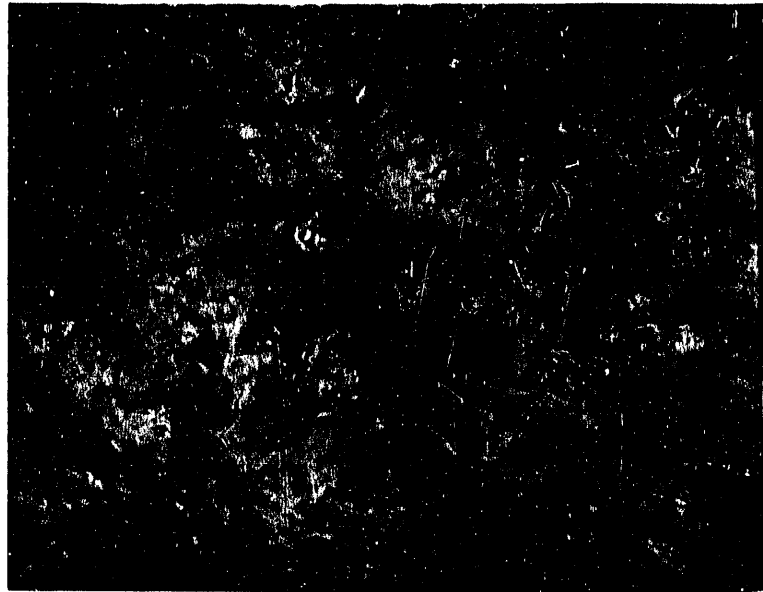
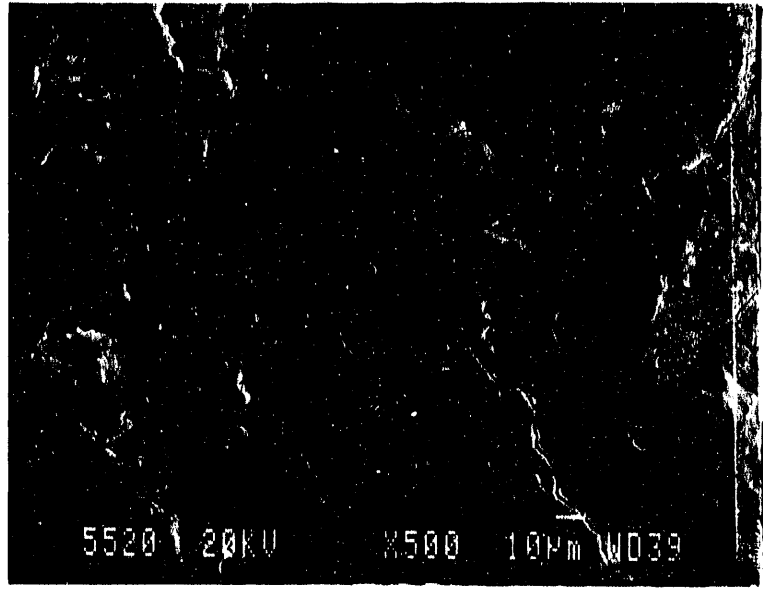


FIGURE 5.6. NCAW Impingement Coupons Exposed to High-Velocity Jets (15 ft/s) Before Oxide Removal (500X). Top photo is of coupon H6 (0.5 min/cycle) and bottom photo is of coupon H5 (4.5 min/cycle).

Figure 5.4 shows the impingement surfaces of the coupons exposed to the low-velocity slurry jet (4 ft/s) during the NCAW test. The top photo is of coupon H2 (0.5 min/cycle) and the bottom photo is of coupon H1 (4.5 min/cycle). No apparent difference in surface condition is observed related to increased exposure time. Finish marks from initial preparation are clearly visible, indicating little erosion of the surface. One feature visible on these specimens and those in Figures 5.5 and 5.6 is the appearance of cracks in the oxide film. This cracking was not evident in the control coupon oxide films (Figure 5.2).

Figure 5.5 shows typical areas of the surfaces of the NCAW test mid-velocity jet impingement coupons before the surface oxide was removed. The specimens still show the original finish marks, although slightly less distinctly than the coupons from the low-velocity jets, indicating slightly higher oxide dissolution and removal under the action of the mid-velocity slurry jet. Again, the cracking is evident in the oxide layers on the specimens in contrast to the control coupon surfaces.

Figure 5.6 shows the surfaces of the NCAW test impingement coupons exposed to the high-velocity jets before the surface oxide was removed. In these photomicrographs one can see significantly more smoothing of the oxide, removing all but traces of the original finish marks from both specimens. This smoothing is an apparent function of jet velocity. Under the high-velocity jet the amount of surface wear corresponds to increased impingement cycle time. Coupon H5 (4.5 min/cycle) appears to be more worn than coupon H6 (0.5 min/cycle). Again, notice the cracks in the oxide. The view of coupon H6, which had the lower exposure time (0.5 min/cycle) but higher weight loss, appears to show larger cracks in the surface oxide in comparison with the other coupons. Spalling of the oxide could partially account for higher weight losses and higher corrosion rates because of the newly exposed or less protected metal surface at the bottom of the cracks.

The following summarizes our observations from the SEM examination of impingement coupon surfaces before the oxide was removed:

- The original surface texture is more evident at the lower jet velocities, similar to the control coupon surfaces. There is little, if any, difference in appearance as a function of impingement cycle time.
- Increasing jet velocity from low- to mid-velocity shows less of the original surface texture, which is consistent with higher weight loss measurements. The mid-velocity coupons still do not show clear differences in surface appearance as a function of impingement cycle time.
- With the high-velocity jet coupons more deterioration of the surface texture is evident. A difference in surface condition as a function of impingement cycle time is apparent with the longer impingement time, resulting in a more worn surface appearance.

Similar SEM characterizations of the surfaces of the NCRW test coupons were not performed.

### 5.3 FINAL TEST RESULTS

Final weight losses were measured after removing the oxide surface layers that accumulated on the sample surfaces as a result of corrosion during the test, and time-averaged base metal corrosion rates were subsequently calculated. The oxides were removed by an inhibited acid cleaning solution (see Section 4.4.3). Since only one measurement per specimen could be made to determine the complete base metal weight loss, this measurement was made only after the intermediate weight loss rates appeared to be approaching a dynamic equilibrium value.

Intermediate weight loss measurements made periodically up to 150 days of exposure indicated that this apparent dynamic equilibrium condition had been approached in the NCAW test. However, it apparently was not reached in the NCRW test. The following sections discuss the results of those final weight measurements made after removal of the oxide films from both the control and the impingement coupons. Actual weight measurements of the coupons are given in the Appendix.

### 5.3.1 Control Coupons

Table 5.3 lists the final weight losses of base metal per unit area for the control coupons following 150 days exposure to the simulated NCAW slurry and 107 days exposure to the simulated NCRW slurry. The preliminary weight losses after final inspection of the same coupons are also given to indicate the amount of oxide film adhering to the coupon surfaces. Calculated final corrosion rates for the control coupons are also listed.

The data for the replicate samples show good agreement in weight losses. The NCAW control coupons had an average weight loss of  $\sim 2.5$  mg/cm<sup>2</sup>, corresponding to a base metal loss in thickness of  $\sim 0.1$  mil during the 150-day test. The NCRW control coupons averaged 1.7 mg/cm<sup>2</sup> over the 107-day test. The average weight losses per unit area were then used for final calculations of corrosion rates for the control coupons and the impingement coupons for the respective tests. Calculated corrosion rates for the control coupons are useful for comparison with corrosion rates measured in other similar tests of

TABLE 5.3. Summary of Data for Control Coupons from NCRW and NCAW Tests

Coupon	Surface Area, cm <sup>2</sup>	Preliminary <sup>(a)</sup> Weight Loss, mg/cm <sup>2</sup>	Final <sup>(b)</sup> Weight Loss, mg/cm <sup>2</sup>	Calculated <sup>(c)</sup> Corrosion Rate, mil/yr
<u>NCRW</u>				
HC1	49.69	-0.33 <sup>(d)</sup>	1.65	0.28
HC2	50.36	-0.22	1.75	0.30
HC3	<u>51.30</u>	<u>-0.22</u>	<u>1.71</u>	<u>0.29</u>
Average	50.45	-0.26	1.70	0.29
<u>NCAW</u>				
H7	51.68	1.20	2.58	0.31
H8	51.58	1.19	2.52	0.31
H9	<u>51.83</u>	<u>1.10</u>	<u>2.37</u>	<u>0.29</u>
Average	51.70	1.16	2.49	0.30

(a) Preliminary weight losses = starting weights - 150-day interim weights (oxide remaining).

(b) Final weight losses = starting weights - final cleaned weights (oxide removed).

(c) Corrosion rate based on final weight losses.

(d) Negative weight loss values (weight gain) indicates accumulation of a corrosion product layer.

carbon steel in simulated waste slurries. For example, in a PNL study of carbon steel corrosion in various types of simulated Hanford-type wastes, corrosion rates of <0.5 mil/yr and generally <0.2 mil/yr were observed under similar conditions (Divine et al. 1985). This agreement provides support for the results obtained from the corrosion test.

Figure 5.7 shows a photomicrograph of a typical surface area from one of the NCAW control coupons after the coupon had been through the cleaning process. Small patches of residual oxide film (darker patches in the photo with light edges) still adhere to the surface of the coupon. The original finish marks are still clearly visible on the surface of the carbon steel. No other surface damage resulting from exposure to the caustic slurry was apparent, indicating that uniform corrosion (as opposed to erosion) is the predominant corrosion mechanism for weight loss from the control coupons.

### 5.3.2 Impingement Coupons

Table 5.4 lists the final adjusted weight losses of base metal and the adjusted time-averaged corrosion rates for the impingement coupons after

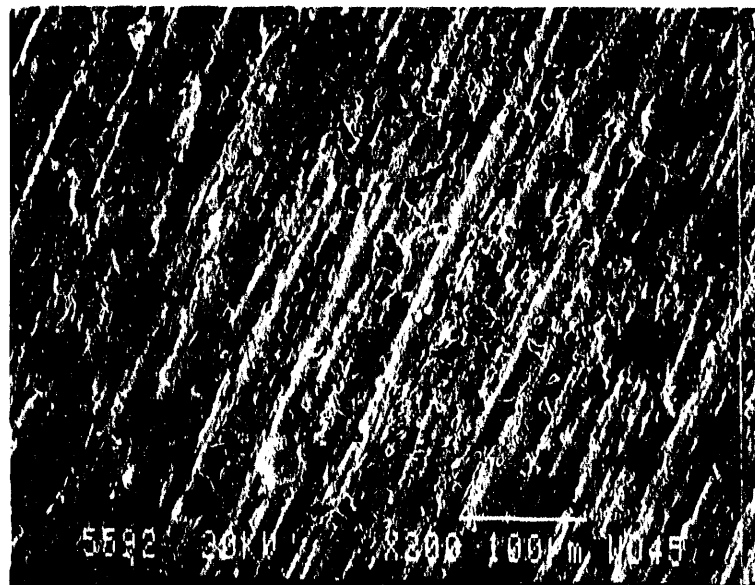


FIGURE 5.7. Typical Surface Area of NCAW Control Coupon Following the Cleaning Process (200X). Photo is of coupon H7 after 150 days exposure to simulated NCAW at ~217°F (103°C). Residual patches of oxide film can be seen on the coupon.

TABLE 5.4. Final Adjusted Weight Losses and Time-Averaged Corrosion Rates for the Impingement Coupons

Coupon <sup>(a)</sup>	Adjusted Weight Loss/Area, mg/cm <sup>2</sup>		Adjusted Corrosion Rate, mil/yr	
	Before Film Removal	Final	Final <sup>(b)</sup>	Time Averaged <sup>(c)</sup>
<u>NCRW</u>				
H1	19.9	23.1	3.40	3.95
H2	12.8	16.3	2.19	2.79
H3	5.1	9.0	0.87	1.54
<u>NCAW</u>				
H1	10.3	17.8	1.26	2.17
H2	5.0	9.7	0.61	1.18
H3	12.0	20.0	1.46	2.44
H4	8.2	14.2	1.00	1.73
H5	15.1	23.2	1.84	2.83
H6	20.3	33.1	2.47	4.04

- (a) Velocity (ft/s): H1 = 54.5; H2 = 14.4; H3 = 3.6.  
 (b) Based on weight change over last intermediate interval.  
 (c) Based on weight change after cleaning to remove oxide film.  
 (d) Velocity (ft/s): H1 = 4; H2 = 4; H3 = 8; H4 = 8; H5 = 15; H6 = 15. Impingement Time (min/5-min cycle): H1 = 4.5; H2 = 0.5; H3 = 4.5; H4 = 0.5; H5 = 4.5; H6 = 0.5.

exposure to simulated NCAW slurry at ~217°F (103°C) for 150 days, and to simulated NCRW slurry at ~180°F (82°C) for 107 days. These adjustments include compensation for the specimen surface areas that were not impacted by the slurry jets. The corresponding weight losses before oxide film removal and the corrosion rates based on the final interim weight changes are shown for comparison. The maximum calculated loss in base metal thickness for the 150-day NCAW test was ~1.6 mil for coupon H6 (high jet velocity/short exposure time).

The comparable NCRW metal loss would be 0.8 mil for coupon H2 (14.4 ft/s) in 107 days, or about 1.2 mil in 150 days assuming a constant rate. This metal loss is observed over an area that is four times as large as that for the NCAW test coupon, an area where the flow characteristics include those of both the impingement region and the radial wall jet region. The

difference in flow characteristics over the test coupons between the two tests is discussed further in Section 6.1, and weakens any conclusions drawn from a comparison between the NCRW and NCAW test results.

## 6.0 DISCUSSION OF RESULTS FROM IMPINGEMENT CORROSION TESTS

This section compares the results of the two impingement tests, and discusses the conclusions and recommendations for improving the tests.

### 6.1 SIMILARITIES AND CONTRASTS BETWEEN NCAW AND NCRW TESTS

The results of the NCAW and NCRW tests must be compared in the context of the similarities and differences between the tests. Table 6.1 summarizes the

TABLE 6.1. Comparison of NCRW and NCAW Corrosion Test Parameters

<u>Test Parameter</u>	<u>NCRW</u>	<u>NCAW</u>
<u>Coupon:</u>		
Shape	disk	disk
Size	3/8- x 1-1/2-in. dia	3/8- x 3/4-in. dia
Material	A-537 carbon steel	A-537 carbon steel
<u>Temperature:</u>	179-182°F	214-216°F
<u>Slurry Jet:</u>		
Distance to coupon	1.5 in.	5 in.
Velocities	3.6, 14.4, 54.5 ft/s	4, 8, 15 ft/s
<u>Slurry Chemistry (supernate):</u>		
pH	>13	>13
OH <sup>-</sup>	0.76 M	1.1 M
NO <sub>3</sub> <sup>-</sup>	0.48 M	2.4 M
NO <sub>2</sub> <sup>-</sup>	0.12 M	--
F <sup>-</sup> , Cl <sup>-</sup> , SO <sub>4</sub> <sup>2-</sup>	0.73 M	0.25 M
<u>Test Duration:</u>	107 days	150 days
<u>Interim Weighing Periods:</u>	7 to 14 days	7 to 41 days
<u>Interim Coupon Treatment:</u>		
Rinse	deionized water	deionized water
Dry	125°C for 60 min and cool in desiccator	110°C for 30 min and cool in desiccator
<u>Control Coupons:</u>		
Material	A-537	A-537
Shape	rectangular	rectangular
Flow conditions	stagnant	stagnant

parameters for both tests. The similarities between the tests include the carbon steel alloy, two of the three slurry jet impingement velocities ( $3.6 \approx 4$  ft/s and  $14.4 \approx 15$  ft/s), slurry chemistry ( $\text{OH}^-$  and  $\text{NO}_3^-$  anions major), slurry pH (~13), and handling procedures for mid- and post-test control and impingement coupons. The differences include size of the carbon steel disk and distance from the slurry jet nozzle, and therefore differences in the slurry flow characteristics over the surface of the coupons; the test temperature ( $180^\circ\text{F}$  for the NCRW test and  $215^\circ\text{F}$  for the NCAW test); the test duration (107 days for the NCRW test and 150 days for the NCAW test); and the presence of nitrite, fluoride, and chloride in the NCRW slurry, compounds that either were not present or were at much different concentrations in the NCAW slurry.

The difference in characteristics of flow over the surface of the NCRW coupons versus flow over the NCAW coupons may be very important. The "free jet" model does not precisely fit the geometry established for the NCRW test, and fits in only a limited sense for the NCAW test. In the NCRW test, the coupon that was situated 1.5 in. from the jet nozzle presented a significant boundary condition not considered in the "free jet" model. The coupon redirected the slurry flow from a normal (perpendicular) axial flow into a radial pattern at the coupon surface. The flow was essentially stagnant at the centerline of the jet. Therefore, the radial component of velocity of the redirected flow would first increase then decrease with radial distance from the centerline. Because of their smaller diameter (0.75 in.) and greater distance from the jet nozzle (5 in.), the NCAW coupons subtended a much smaller solid angle than did the larger and more closely positioned NCRW coupons. Because of the distance from the nozzles to the coupons and the smaller coupon diameter, the overall flow patterns of the slurry jet in the NCAW test were probably closer to that of a free jet. However, the slurry flow pattern over the surface of the NCAW coupons still should have been similar to that for the NCRW coupons, except that the radial velocity distribution across the NCAW coupons would be similar to that for a small central region on the NCRW coupons. The point is that NCRW coupons probably directly compare with the NCAW coupons over only a very small area, and until the actual slurry velocity profiles are known with some certainty, more accurate comparisons between the two tests cannot be made.

An evaluation of the coupon positioned out of the direct impingement of the jet (the off-jet position) in the NCAW test revealed another difference in the flow characteristics between the two tests. Originally, it was thought that the coupon in the off-jet position was essentially not exposed to any fluid flow, similar to the environment of the control coupons. However, as shown schematically in Figure 6.1, the diverging jet spills over the edge of the direct impingement coupon and flows in a turbulent, oblique current over the coupon in the off-jet position. Hence, the NCAW test was not an "on-off" test, but was instead a comparison of the effects of two kinds of flows, direct impingement and an uncharacterized oblique flow. Therefore, it is believed that the NCAW coupons were exposed to a flow condition that did not occur in the NCRW test, and in either case flows impinging on the test coupons have not been representative of all the slurry flow patterns that will occur across the tank walls during retrieval operations.

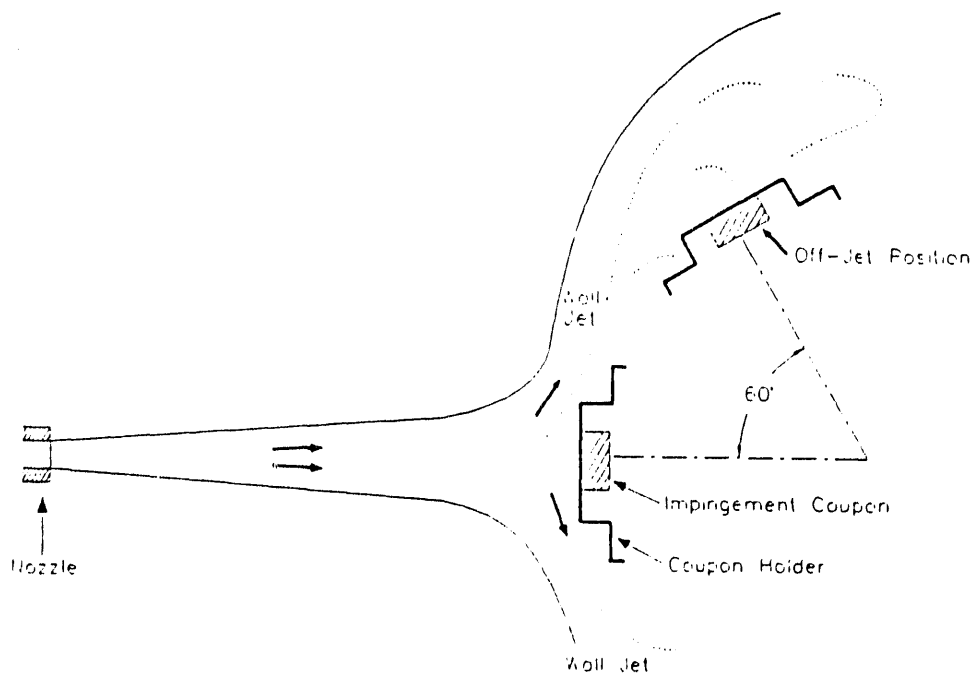


FIGURE 6.1. Probable Flow Pattern for NCAW Slurry Jet. Specimen holder geometry and off-jet position directs turbulent, oblique flow over the off-jet position.

In addition, differences in test temperature, slurry composition, and slurry impingement velocity distribution make a direct comparison between the two tests uncertain. Test temperature likely had some effect on the corrosion rate in both slurry systems, while the differences in slurry composition may have little or no effect. The distribution in slurry impingement velocity across the coupon could make a difference in the actual corrosion rate across the surface of the NCRW test coupons. However, we surmise from the results of the NCAW tests (see further discussion below) that while vertical velocity in the impingement region affected corrosion rate, redirected flow in the off-jet position apparently caused increased corrosion compared to stagnant conditions. Further efforts to measure changes in thickness of the NCRW coupons before and after the NCRW test found the relative change in thickness to be less than 1 mil, suggesting that any differences in corrosion rate between the edge and center of the NCRW coupons were less than about 3 mil/yr (i.e., differences in the corrosion rate from center to edge were less than a factor of ~2).

## 6.2 SIMILARITIES AND CONTRASTS BETWEEN NCRW AND NCAW TEST RESULTS

Table 6.2 lists some of the important results from the two tests. The first column lists the amount of corrosion film removed from each test coupon after the tests were terminated. Note that the NCAW impingement coupons showed a considerably thicker buildup of film than did the NCRW coupons. The control coupons showed the opposite condition (the NCRW controls showed a 50% thicker film than did the NCAW controls). Column 2 indicates the amount of metal that was lost per square centimeter from each coupon. From that the total amount of film formed, assuming magnetite was the final film phase, can be calculated (see column 4). In every case, with the exception of the NCRW control coupons, considerably more film-forming components have gone into solution (column 4) than have remained on the coupons as film (column 1).

Figures 6.2 and 6.3 show the relationships between the velocity of the slurry jet, the time-averaged corrosion rates, the adhering oxide film mass, and the mass of corrosion products removed in solution during the course of the experiment. These correlations were made to emphasize similarities and

TABLE 6.2. Summary of Results from NCRW and NCAW Corrosion Tests

Coupon	Test Result <sup>(a)</sup>						
	1	2	3	4	5	6	7
<u>NCRW</u>							
H1	3.28	23.14	31.93	28.65	3.95	54.5	100
H2	3.52	16.28	22.47	18.95	2.78	14.4	100
H3	3.87	8.97	12.38	8.51	1.53	3.6	100
HC1	1.98	1.65	2.28	0.30	0.28	0	--
HC2	1.97	1.75	2.42	0.45	0.30	0	--
HC3	1.93	1.71	2.36	0.43	0.29	0	--
<u>NCAW</u>							
H1	7.59	17.72	24.45	16.86	2.18	4	90
H2	4.73	9.70	13.39	8.66	1.18	4	10
H3	7.90	19.92	27.49	19.59	2.44	8	90
H4	6.00	14.19	19.58	13.58	1.73	8	10
H5	8.08	23.16	31.96	23.88	2.82	15	90
H6	12.84	33.14	45.73	32.89	4.04	15	10
H7	1.38	2.58	3.57	2.19	0.31	0	--
H8	1.33	2.52	3.48	2.15	0.31	0	--
H9	1.27	2.37	3.27	2.00	0.29	0	--

(a) Column	Description
1	Weight of corrosion film at end of test (mg/cm <sup>2</sup> )
2	Weight of metal removed by corrosion (mg/cm <sup>2</sup> )
3	Weight of total corrosion product (mg/cm <sup>2</sup> ) = Fe <sub>3</sub> O <sub>4</sub> (wt. Fe x 1.38)
4	Weight of corrosion product dissolved during test (mg/cm <sup>2</sup> )
5	Time-averaged corrosion rate (mil/yr)
6	Slurry jet impingement velocity (ft/s)
7	Percent of time in slurry jet out of a 5-min cycle

differences between the various test results and to suggest relationships not already recognized. The pre-cleaning values (see Table 5.4) were found to be well correlated to the post-cleaning corrosion values, so both sets of corrosion rates show the same relationship to velocity and other data. Therefore only one set needs to be analyzed this way.

Figure 6.2 plots the time-averaged corrosion rates (rates based on total weight loss of metal as determined at the end of the test) versus the free jet velocity calculated for the impingement surface (see Section 3.3). The curves

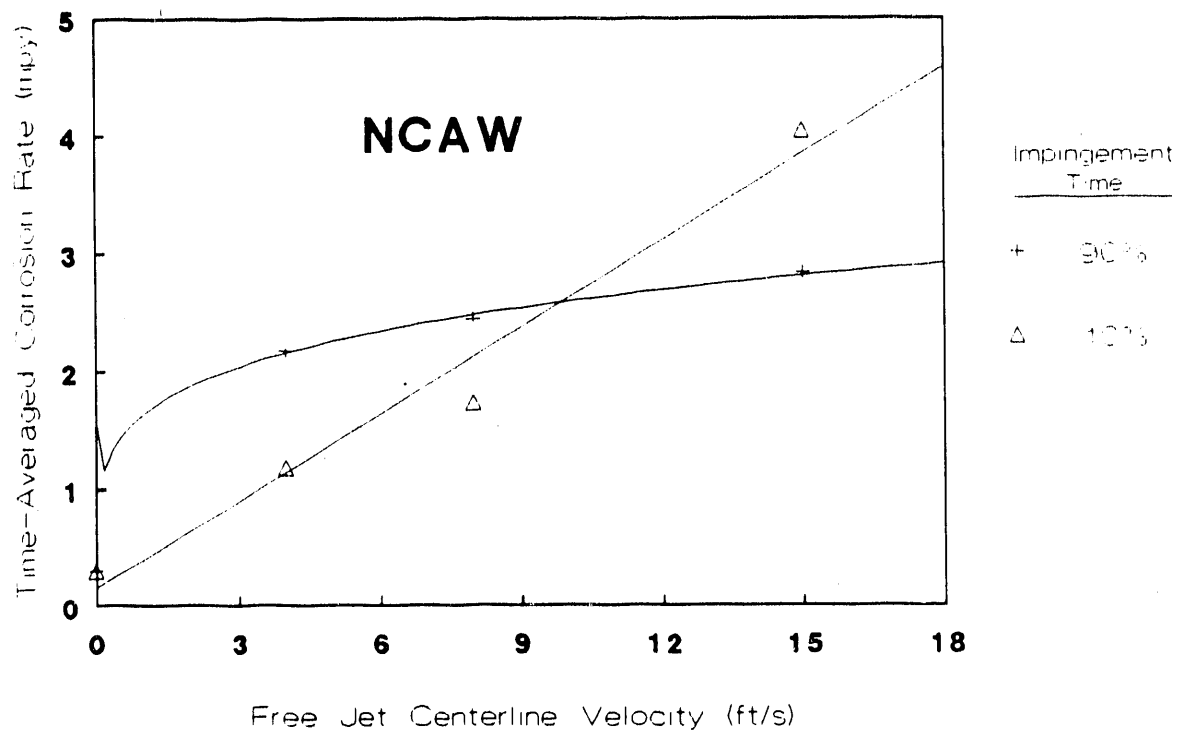
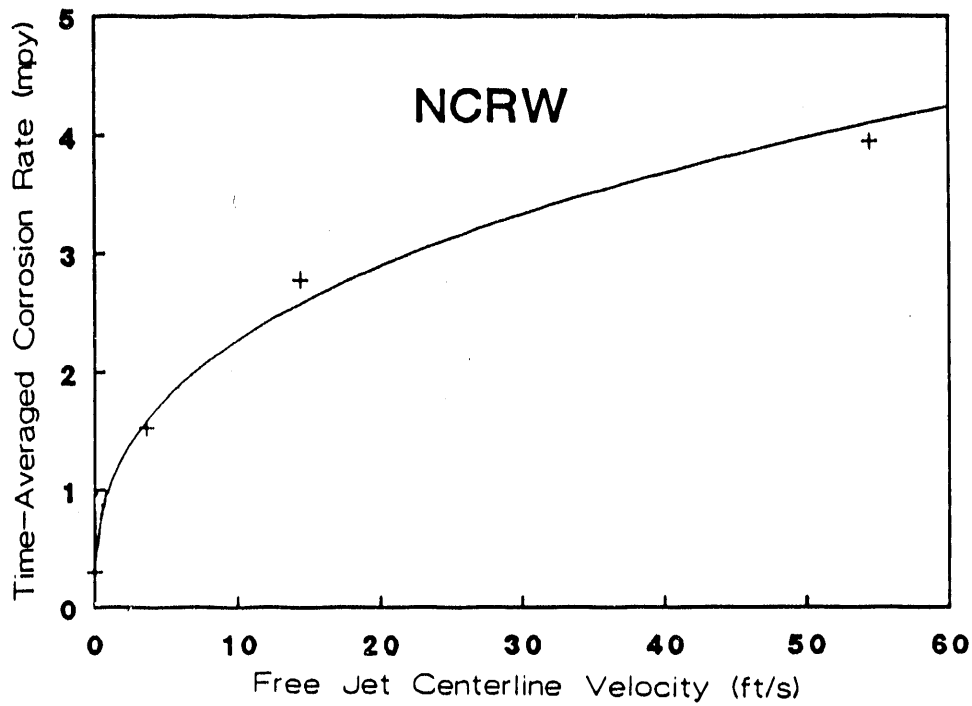


**FIGURE 6.2.** Post-Cleaning Corrosion Rates as a Function of Jet Velocity. Velocities shown are those of free jet centerlines at a scaled distance from the test nozzle equivalent to the distance from the mixer pump nozzle to the tank wall.

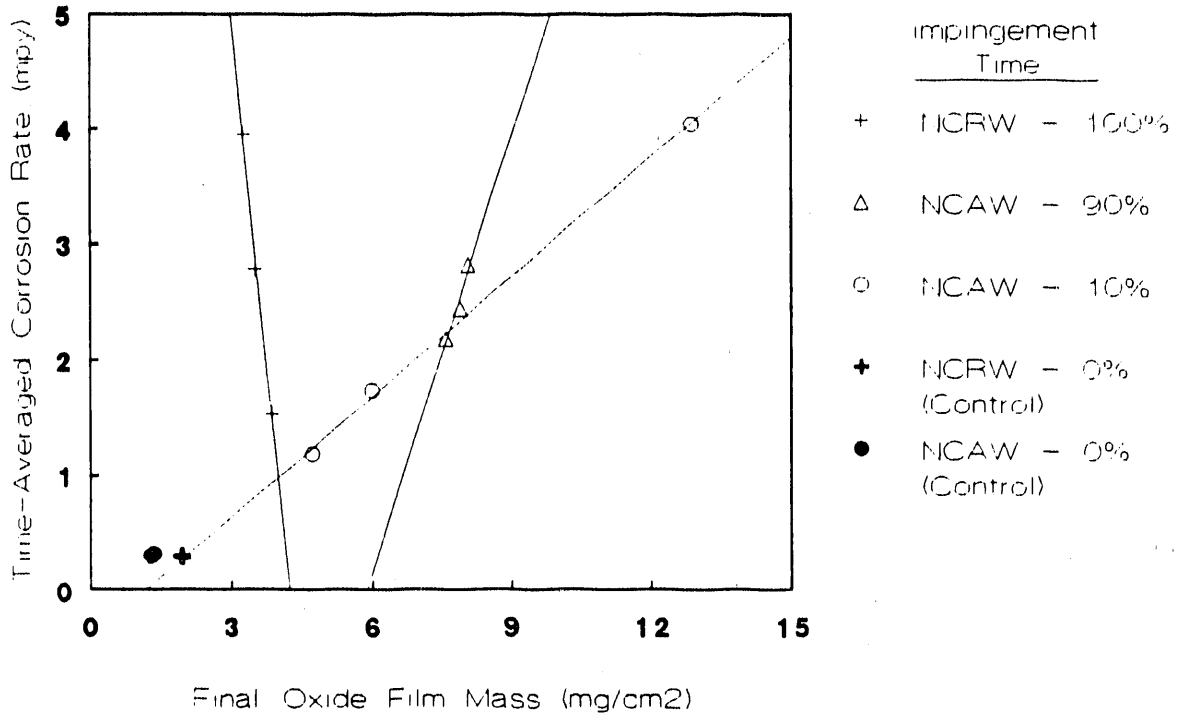


**FIGURE 6.3.** Correlation of Time-Averaged Corrosion Rates (Based on Weight Change, Including Cleaning) with Oxide Film Mass

for both the NCRW and NCAW tests (90% impingement time) appear to show corrosion rates that are approximately proportional to the square root of the slurry velocity. This is consistent with the expectation that the impingement zone of a circular jet striking a wall would show mass transfer characteristics proportional to the square root of the impinging slurry velocity. However, the corrosion rates displayed by the coupons that were out of direct impingement 90% of the time were linearly proportional to the slurry velocity. This result suggests a boundary layer control on the corrosion rate for those cases (see Section 3.3).

Figure 6.3 correlates the final oxide film mass on the specimen with the time-averaged corrosion rate for that specimen. The NCRW and NCAW test results appear to be distinctly different on this plot. Here, the NCAW coupons that spent most of the time out of the direct flow from the slurry jets show a linearly increasing oxide film thickness with increasing corrosion

rate. This indicates that the film thickness could not be the rate-determining factor for these coupons; rather, the film forms at a rate that is proportional to the corrosion reaction. It is interesting to note that the control coupons lie on the same trend, suggesting that most of the film must be quite porous to the corroding species for such lack of control. The NCRW coupons show almost the opposite correlation. Here, the thickest film is on the slowest corroding coupon, but the variation in thickness may not be significant. The 90% direct impingement NCAW coupon seems to form a third independent trend that looks like it is in transition from the 10% direct impingement mode to that displayed by the NCRW coupons. Note that the NCAW impingement films were cleaned off in the same time it took to remove the much thinner films on the control coupons. Lack of information regarding the phases present in the films, their porosity, and the surface appearance of the NCRW coupons makes further speculation unwarranted, beyond our observation that there are significant differences between the oxide films on the two sets of test coupons.

The differences between the tests may be attributed to chemistry, temperature differences, flow patterns, or length of the experiment (i.e., the NCAW test, which ran about 50% longer, may have reached an equilibrium state that the NCRW test did not reach). For example, temperature affects the conversion of iron hydroxide into magnetite, and magnetite should produce a more durable film than would iron hydroxide. The more massive film in the NCAW test could be due to a higher proportion of magnetite in the film. Magnetite may also produce a more porous film because of recrystallization, and may explain why the film thickness did not appear to be the controlling factor for corrosion rate on these coupons. Overall, it appears from the film-forming characteristics that two distinctly different test conditions were represented, and that the similarities of the time-averaged corrosion rates for similar slurry impingement velocities (see column 5 in Table 6.2) are merely coincidental.

### 6.3 INTERPRETATION OF INTERIM WEIGHT CHANGE OBSERVATIONS

Figures 6.4 and 6.5 provide another comparison of the results of these two tests. In these figures the corrosion rates plotted are based on the net weight change observed between interim weighings. As already discussed in Section 5.1.2, the net weight change is the sum of the weight of the metal lost from the coupon's surface and the change in weight of the corrosion film adhering to the surface. While the metal lost due to corrosion is always negative, the change in weight of the corrosion film can be either positive or negative. Hence, the measured weight change is an indeterminate number that can be assumed equal to the metal actually lost from corrosion, if there is reason to believe that the corrosion film on the coupon surface is unchanging or changing slowly in mass per unit area compared to the actual corrosion rate.

The measured weight loss rates computed for the control coupons and plotted in Figure 6.4 indicate for the NCAW controls that the corrosion film may have stabilized as corrosion progressed, as indicated by the fact that the corrosion rate based on observed weight change becomes constant and is positive. In this case the coupon is losing mass. The loss of mass can be attributed to the loss of metal without a concurrent increase in the corrosion film mass (the corrosion products go directly into solution). However, as long as the calculated corrosion rate is negative (as is observed for the NCRW control coupons), the corrosion film has to be growing in mass per unit area since the loss of metal to corrosion will cause only a weight loss, while increasing the amount of corrosion film adhering to the coupon will cause a weight gain (i.e.,  $Wt(Fe_3O_4) = 1.38 \times Wt(Fe)$ ). Hence, in the case of the NCRW test, the thickness of the oxide film on the control coupons increased throughout the test, but the film on the NCAW control coupons may have stopped growing at a significant rate toward the end of the test.

It appears from Figures 6.4 and 6.5 that, based on weight loss rate, the behavior of the impingement coupons and control coupons reached a similar steady-state condition by the end of the test. The rates for NCAW tests can be generally characterized as rising to a maximum in the first 50 days and then falling over the next 100 days to lower, more constant rates. Note,

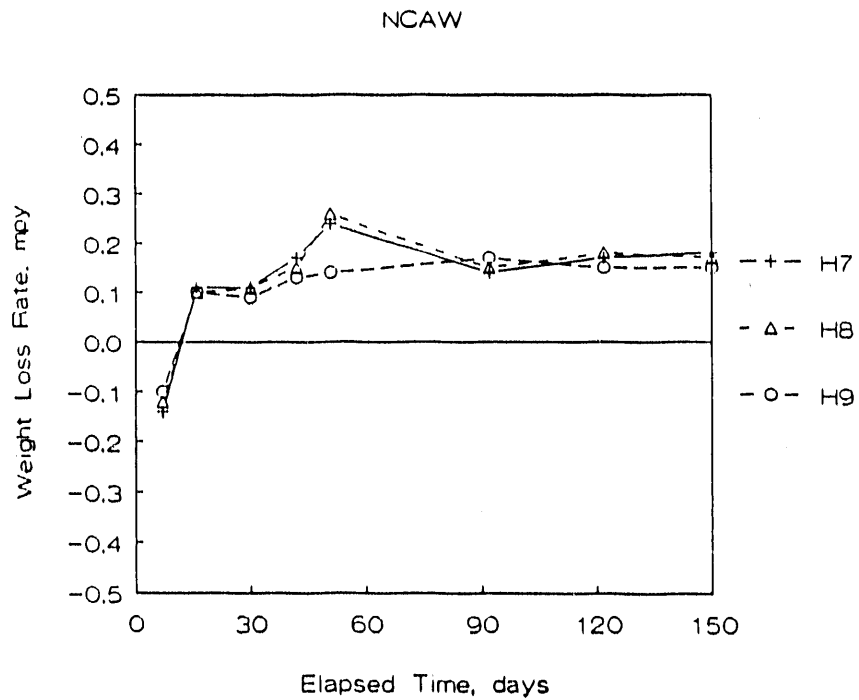
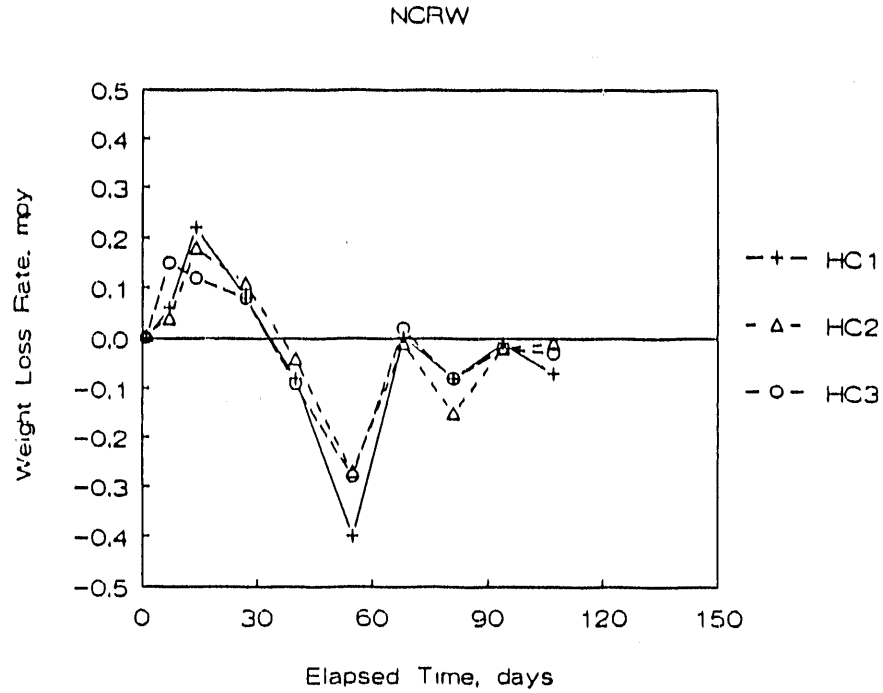


**FIGURE 6.4.** Plots of Measured Weight Loss Rates for the Control Coupons from the NCAW and NCRW Corrosion Tests. Weight loss rate is in terms of equivalent metal loss in mils per year. Negative weight loss rate indicates weight gain.

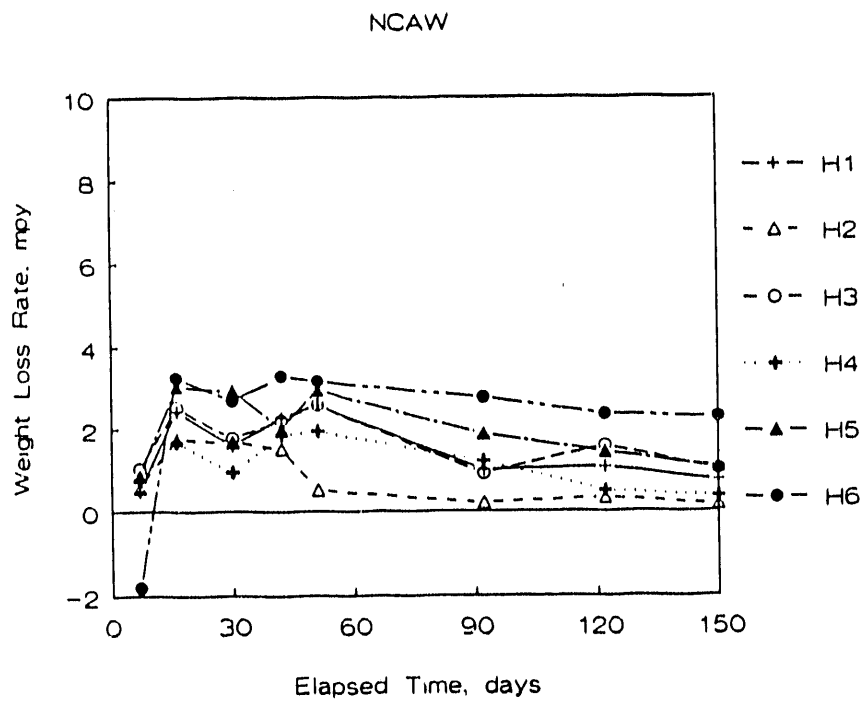
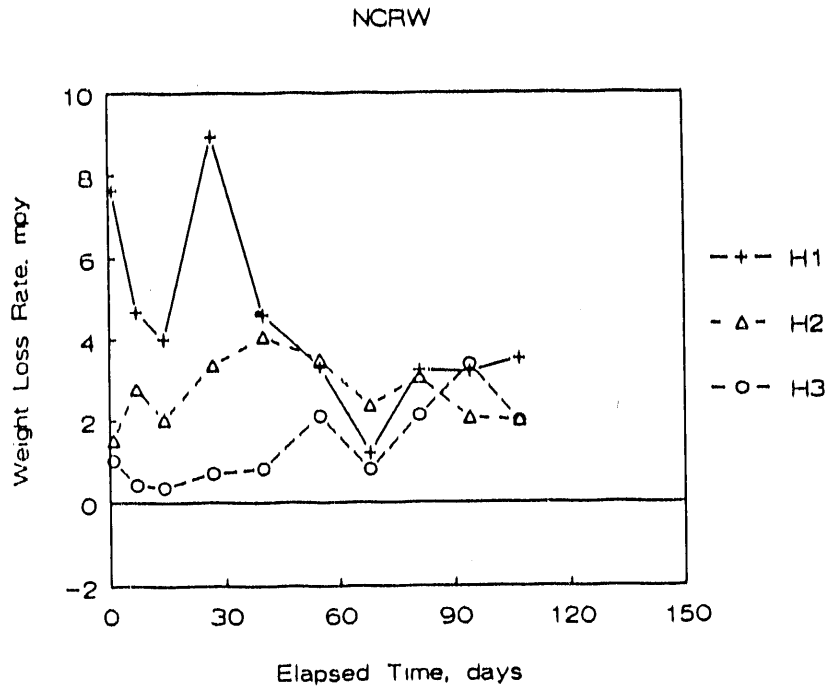


FIGURE 6.5. Plots of Measured Weight Loss Rates for the Impingement Coupons from the NCAW and NCRW Corrosion Tests.

however, that the rates calculated for these impingement coupons are still changing toward lower values, particularly for coupons H1, H3, and H5, so the coupons do not yet appear to be at equilibrium in contrast to the control coupons. By comparison, the NCRW impingement coupons appear to be in a dynamic nonequilibrium state. The calculated values vary almost randomly, and while the measured weight loss rate for the coupon in the highest velocity slurry jet (coupon H1) appears to be falling on the average, the measured weight loss rate for the coupon in the lowest velocity jet (coupon H3) appears to be increasing with time. This is consistent with the behavior shown by the NCRW control coupons, in that they too were still in transition after 107 days.

Another consistency in rates for the NCAW and NCRW tests is shown by the relationship between the time-averaged corrosion rate (see Table 6.2) and the measured weight loss rate. For the NCAW test, the time-averaged rate is generally greater than or equal to the greatest measured weight loss rate. This is what one would expect when a thick corrosion film forms during the test so that the weight loss of metal is partially compensated by film buildup. A relatively thick film developed on the NCAW test coupons. In the NCRW case, the time-averaged value (see Table 6.2) is always less than the greatest measured weight loss rates observed in every case. This implies that, on the average, the corrosion film was a smaller component of the system, which is again consistent with the relatively thin film on the NCRW test coupons. The thickness of the corrosion film may have changed considerably during the course of the test, thus explaining the apparent increasing corrosion rate on the NCRW test coupon (coupon H3).

The test data as shown in Figure 6.5 suggest the following conclusions. The NCRW results are best represented as the time-averaged corrosion rates given in Table 6.2, because the rates did not appear to have reached a stable condition by the end of the test. Therefore, the more conservative value for velocity-accelerated corrosion rate is recommended. The NCAW test results show that the rates are more well behaved, although apparently are still approaching a steady-state condition (i.e., the observed weight changes are still decreasing with time). It is probably accurate to state that the time-averaged corrosion rates given in Table 6.2 for the NCAW coupons overestimate

the actual corrosion rate occurring at the end of the test. Caution is advised in saying how much the time-averaged values overestimate the true corrosion rate. Weight changes in the relatively thick corrosion film considerably alter the meaning of the measured weight loss rate, but that effect would not be detected by the measurements made during the tests.

Another observation is that the corrosion rates for the NCRW slurry appear to be higher than those for the NCAW slurry. This observation is based on the conclusion that the time-averaged rate for the NCRW appears to be the best estimate of the actual corrosion rate, while the best estimate for the NCAW rates were based on the measured weight loss rates determined at the end of the NCAW test. Combining this observation with the fact that the NCRW test was run at a lower temperature than the NCAW test supports the conclusion that the simulated NCRW slurry was more corrosive than the simulated NCAW slurry under equivalent conditions.

#### 6.4 CONCLUSIONS AND RECOMMENDATIONS FOR FUTURE TESTS

The following conclusions can be drawn from the NCAW/NCRW test results:

- Based on variability in the data, corrosion rates for A-537 carbon steel under the NCRW test conditions are best estimated using the time-averaged values presented in Table 6.2.
- Corrosion rates for A-537 carbon steel under the NCAW test conditions are probably lower than the time-averaged values presented in Table 6.2. The corrosion rates based on net weight change (see Figure 6.3) may be a good estimate (2.5 mil/yr) of the actual value for the highest rate in the NCAW slurry (see Table 5.4). These values need to be confirmed by a test designed for this purpose.
- The A-537 carbon steel behaved differently in the two slurries based on film thicknesses. Slurry composition may have been the factor.
- Bulk flow of the slurry past the coupons in the "off-jet" positions appears to have accelerated corrosion during the NCAW test. The actual flow pattern is not known but is probably due to turbulent flow generated by the slurry jet as it is redirected by the impingement coupon aligned with the jet (see Figure 6.1).

- The difference in flow pattern and velocities across the surface of the NCRW test coupons did not produce a measurable difference (~3 mil/yr) in corrosion rate between the center and the edge of the coupons.

The following recommendations are made for future work and test design:

- Future tests should be designed so that multiple samples are tested under identical conditions. This approach will allow actual corrosion rates to be determined and data reproducibility to be measured.
- Future tests should eliminate interim measurements in which the inspected coupons are returned to the test slurry. Such activity creates some uncertainty about the results because the coupons are handled during the procedure, and the potential for mechanically stressing the corrosion film when it is exposed to another environment (i.e., deionized water), allowed to dry, and then rewetted is unknown.
- A matrix of scoping tests should be developed in parallel with the main testing program to specifically investigate the effects of slurry composition on corrosion rate. Ideally, the whole compositional grid could be run in parallel. The compositional grid would cover variations in OH, NO<sub>2</sub>, NO<sub>3</sub>, and potential iron complexing agents.
- Tests should be designed so that the test coupons are always in a well-defined environment with respect to slurry motion. The slurry motion should be hydrodynamically scaled to closely match the magnitude and types of motion expected in the double-shell tanks. This scaling will be done in the test tank by placing a rotating jet at the center of the tank and using a test coupon holder scaled to act as a section of the DST tank wall as a source for impingement by the mixer pump jets. This test configuration can be scaled to produce test conditions that match the impingement angles, impingement velocities (and wall shear), and cycle times characteristic of planned DST operations. One or more jet velocities, scaled to that anticipated in the DSTs, would be tested.
- Test specimens should be preconditioned for any test. The object of such preconditioning would be to produce a specimen surface that closely reproduces that on the inner surface of the tank. Preconditioning would include the following three steps:
  - Give each test coupon a standard surface finish.
  - Heat treat the test coupons in the same way that the tank was heated, thus producing an oxide film similar to that produced in the tank.

- Precondition the test coupons in a generic tank supernatant solution at the same temperature to be used in the test. The treatment should be long enough so that the initial transient corrosion rates associated with bare metal coupons are eliminated or significantly reduced. Several coupons should be characterized to provide a well-defined, initial-state baseline for comparison to test results.

## 7.0 REFERENCES

- Anantatmula, R. P. 1990. Hanford Site Environmental Restoration and Waste Management Technology Plan: Calendar Year 1990. WHC-EP-0212-1, Westinghouse Hanford Company, Richland, Washington.
- ASTM. 1985. Annual Book of ASTM Standards. "Erosion and Wear; Metal Corrosion." Vol. 03.02, American Society for Testing and Materials, Philadelphia, Pennsylvania.
- Beltaos, S., and N. Rajaratnam. 1974. "Impinging Circular Turbulent Jets." Journal of the Hydraulics Division, Proc. of the Amer. Soc. of Civil Eng. 100(HY10):1313-1327.
- Brubaker, G. R., and P.B.P. Phipps, eds. 1979. Corrosion Chemistry. ACS Symposium Series 89, American Chemical Society. Washington, D.C.
- Chia, C., F. Giralt, and O. Trass. 1977. "Mass Transfer in Axisymmetric Turbulent Impinging Jets." Ind. Eng. Chem., Fundamentals. 16(1):28-35.
- Cragolino, G., C. Czajkowski, and W. J. Shack. 1988. Review of Erosion-Corrosion in Single-Phase Flows. NUREG/CR-5156, ANL-88-25. Argonne National Laboratory, Argonne, Illinois.
- Divine, J. R., W. M. Bowen, D. B. Mackey, D. J. Bates, and K. H. Pool. 1985. Prediction Equations for Corrosion Rates of A-537 and A-516 Steels in Double Shell Slurry, Future PUREX, and Hanford Facilities Wastes. PNL-5488, Pacific Northwest Laboratory, Richland, Washington.
- Fontana, M. G., and J. D. Greene. 1978. Corrosion Engineering. 2nd Ed. McGraw-Hill Book Company, New York.
- Giralt, F., C. Chia, and O. Trass. 1977. "Characterization of the Impingement Region in an Axisymmetric Turbulent Jet." Ind. Eng. Chem., Fundamentals. 16(1):21-28.
- Perry, R. H. 1963. Chemical Engineers Handbook. 4th Ed. McGraw-Hill Book Company, New York.
- Rajaratnam, N. 1976. Turbulent Jets. Elsevier, New York.
- Sanchez-Caldera, L. E., P. Griffith, and E. Rabinowicz. April 1988. "The Mechanism of Corrosion-Erosion in Steam Extraction Lines of Power Stations." Journal of Engineering for Gas Turbines & Power 110:180-184.
- Schikorr, G. Z. 1933. Anorg. Allg. Chem. 212:533.
- Schlichting, H. 1960. Boundary Layer Theory. 4th Ed. McGraw-Hill Book Company, New York.

Tani, I., and Y. Komatsu. 1966. "Impingement of a Round Jet on a Flat Surface." Proc. of the 11th Intern. Cong. of Applied Mechanics, Munich, 1964. Ed. Henry Görtler. Springer-Verlag, New York.

Zarembo, V. I., A. A. Slobodov, V. G. Kritskii, L. V. Puchkov, and V. M. Sedov. 1986. Thermodynamic Analysis of Coolant Behavior in a Boiling Water Reactor on the Basis of the Solubility of the System  $Fe_3O_4$ - $H_2O$ - $O_2$ . Translated from Zhurnal Prikladnoi Khimii, 59(5):1030-1036.

APPENDIX A

COUPON DIMENSIONS AND WEIGHT MEASUREMENTS

APPENDIX A

COUPON DIMENSIONS AND WEIGHT MEASUREMENTS

TABLE A.1. Coupon Weights Measured at Each Inspection Period for the NCRW Corrosion Test

Days from Start	Impingement Coupons			Control Coupons		
	H1	H2	H3	HC1	HC2	HC3
0	84.5439	84.6541	84.7920	117.3469	120.3804	123.2461
0.77	84.5391	84.6441	84.7913	117.3469	120.3801	123.2460
6.77	84.5210	84.6331	84.7891	117.3459	120.3794	123.2435
13.77	84.5020	84.6228	84.7860	117.3417	120.3759	123.2411
26.70	84.4284	84.5941	84.7789	117.3387	120.3721	123.2382
39.63	84.3923	84.5623	84.7734	117.3415	120.3736	123.2416
55.30	84.3672	84.5355	84.7597	117.3578	120.3847	123.2532
68.30	84.3575	84.5164	84.7532	117.3577	120.3852	123.2526
81.30	84.3330	84.4933	84.7377	117.3604	120.3905	123.2556
93.90	84.3073	84.4769	84.7106	117.3606	120.3912	123.2565
106.90	<u>84.2794</u>	<u>84.4614</u>	<u>84.6952</u>	<u>117.3632</u>	<u>120.3916</u>	<u>123.2567</u>
Final <sup>(a)</sup>	84.2421	84.4214	84.6572	117.2649	120.2922	123.1583

(a) Oxide removed.

TABLE A.2. Coupon Weights Measured at Each Inspection Period for the NCAW Corrosion Test

Days from Start	Impingement Coupons									Control Coupons		
	H1	H2	H3	H4	H5	H6	H7	H8	H9			
0	20.9875	21.0753	21.1076	20.9874	20.9467	21.0867	121.3404	121.2907	122.0228			
7	20.9870	21.0747	21.1065	20.9866	20.9458	21.0887	121.3431	121.2930	122.0247			
16	20.9843	21.0722	21.1029	20.9842	20.9415	21.0841	121.3402	121.2910	122.0221			
30	20.9801	21.0678	21.0983	20.9814	20.9344	21.0775	121.3358	121.2867	122.0186			
42	20.9750	21.0641	21.0933	20.9771	20.9298	21.0705	121.3301	121.2816	122.0142			
51	20.9704	21.0624	21.0887	20.9734	20.9247	21.0651	121.3240	121.2751	122.0095			
92	20.9611	21.0581	21.0799	20.9627	20.9098	21.0445	121.3007	121.2578	121.9903			
122	20.9537	21.0542	21.0701	20.9580	20.9007	21.0311	121.2930	121.2425	121.9778			
150	20.9482	21.0512	21.0634	20.9542	20.8938	21.0189	121.2784	121.2293	121.9658			
Final (a)	20.9152	21.0263	21.0295	20.9258	20.8594	20.9709	121.2069	121.1608	121.9001			

(a) Oxide removed.

DISTRIBUTION

<u>No. of Copies</u>		<u>No. of Copies</u>
	<u>OFFSITE</u>	32 <u>Pacific Northwest Laboratory</u>
12	DOE Office of Scientific and Technical Information  S. Agnew Los Alamos National Laboratory P.O. Box 1663 Los Alamos, NM 87545	C. R. Allen R. T. Allemann J. M. Alzheimer J. A. Bamberger J. M. Bates M. R. Elmore (10) L. M. Liljegren N. J. Lombardo P. J. Lowery J. L. McElroy J. M. Perez M. R. Powell P. A. Scott H. D. Smith R. E. Westerman G. A. Whyatt B. M. Wise Publishing Coordination Technical Report Files (5)
5	West Valley Nuclear Services Co. P.O. Box 191 West Valley, NY 14171-0191 ATTN: S. M. Barnes B. P. Bauer R. A. Humphrey J. M. Pope C. M. Schiffhauer	
6	Savannah River Laboratory Westinghouse Savannah River Company Aiken, SC 29801 ATTN: R. G. Baxter P. D. d'Entremont J. M. Fazio J. G. Glasscock J. R. Knight B. Lewis	18 <u>Westinghouse Hanford Company</u>  J. N. Appel W. B. Barton J. S. Garfield G. J. Gauck D. T. Heimberger M. J. Horhota N. W. Kirch E. H. Kohlman W. C. Miller K. B. Sowa L. C. Stegen D. D. Wanner E. D. Waters J. A. Yount Document Clearance Administration (2) Project W151 Files (2)
	<u>ONSITE</u>	
4	<u>DOE Richland Operations Office</u>  M. Dev R. E. Gerton (2) G. W. Rosenwald	

**END**

**DATE  
FILMED**

**4 / 09 / 92**

